NTNU

Norwegian University of
Science and Technology

Modeling of Compressor Characterisics and Active Surge Control

Torbjørn Sønstebø Grong

Master of Science in Engineering Cybernetics
Submission date: June 2009
Supervisor: Ole Morten Aamo, ITK

Norwegian University of Science and Technology
Department of Engineering Cybernetics

Problem Description

Compressor characteristics are an important part of the behavior of a compressor. This data is normally given in data sheets from the manufacturer, but can be very useful to implement in a control system for monitoring and testing, as well as for research.

Active surge controllers are a popular field in the process of new and improved surge controllers for industrial compressors. But despite much research in the field, an active surge controller has yet to be implemented on a commercially available compressor.

- Review different ways of modeling compressor characteristics for simulations in MATLAB.
- Test the simulation friendliness/effectiveness of the different models.
- Present two different solutions for active surge controllers, namely close coupled valve and drive torque actuation.
- Based on the presentation of the active surge controllers, enlighten current problems with the controllers, choose the most promising one and suggest possible solutions for the problems.

Assignment given: 19. January 2009
Supervisor: Ole Morten Aamo, ITK

Abstract

In this thesis, the compressor characteristics, being representations of the compressor pressure ratio as a function of the gas flow through the compressor, have been studied. Three different types of representations of the compressor characteristics are presented, implemented and tested with respect to simulation friendliness and effectiveness. These are based on a physical model, a 4^{th}-order polynomial approximation method and a table lookup method. In addition, two different types of active surge controllers have been critically reviewed, i.e. the Close Coupled Valve (CCV) and the Drive Torque Actuation, and subsequently implemented and tested in SIMULINK.

Based on the tests carried out on the compressor characteristics it is concluded that the 4^{th}-order polynomial approximation method works best in an online environment. On the other hand, the table lookup method provides better representation of the actual data, but the method is somewhat slower compared to the other one. The usefulness of the physical model is limited, but together with parameter identification its applicability can be extended. Moreover, the active surge controllers have proved to be mathematically stable and shown to perform adequately. However, both face a problem with regard to measurement delay. Based on simulations and other considerations, the indications are that the drive torque actuation is the most promising solution for active surge control and should thus be the focus for further investigations. A possible solution for the measurement delay problem is to use a state observer. As a part of the thesis, two state observers have been implemented and tested, but with limited success.

Preface and Acknowledgments

This thesis is the result of my diploma work during the 10^{th} semester of my M.Sc studies in Engineering Cybernetics. First of all I would like to thank Professor Ole Morten Aamo at the Department of Engineering Cybernetics (ITK) at the Norwegian University of Science and Technology (NTNU) for his willingness to act as a supervisor for this project, and Professor Jan Tommy Gravdahl at the same department for discussions about active surge controllers. During the course of the work, a number of other persons have also contributed. In particular, I would like to acknowledge the contributions from my co-supervisor Dr. Fredrik Dessen, Dr. Tu Duc Nguyen and the rest of the staff at Siemens Oil and Gas Offshore, Technology and Innovation, Trondheim. Finally, I am grateful to my parents Professor Øystein Grong and Torhild Sønstebø Grong for their support and encouragements in all respects.

Torbjørn Sønstebø Grong

June 2009, Trondheim, Norway

Contents

List of Figures

Chapter 1

General introduction

1.1 Scope of work

In this thesis, different ways of representing compressor characteristics will be presented and tested. The compressor characteristics are representations of the compressor pressure ratio as a function of the gas flow through the compressor. The compressor characteristics give valuable information about the performance of the compressor. In addition, two different active surge controllers are studied. Compressor surge is a phenomenon that can be very damaging for the compressor and the adjacent processing equipment, and is something one must avoid. Active surge control differs from regular surge control in that instead of operating the compressor at a safe limit away from the point of surge, it seeks to stabilize the compressor within the unstable region. In modern industrial compressor systems, a recycle valve is used for surge control, diverting gas from the compressor outlet back to the inlet in order to maintain a sufficient flow. According to (McKee et al., 2000), approximately 5% of the operating time of a compressor involves recycled flow, which means that about 1% of the fuel being consumed in the compressor is superfluous. The following objectives are the focus of this thesis:

- Review three different methods for approximating the compressor characteristics supplied by the manufacturer. The methods are based on a physical model, a polynomial approximation method and a table lookup method.

- Implement the three different methods in MATLAB, and test them with respect to simulation friendliness and effectiveness.

- Present two different types of active surge controllers, that is Close Coupled Valve(CCV) and Drive Torque Actuation.

- Implement the two controllers in SIMULINK, and then test their performance as well as enlighten the current problems associated with them.
- Based on the above tests and further considerations, choose the most promising solution, which then should be the focus for further research. In addition, attempts will be made to suggest possible solutions for the current problems related to the use of the controller.

1.2 Classification and use of compressors

(Nisenfeld, 1982) classifies compressors into four different general types: reciprocating, rotary, centrifugal and axial compressors.

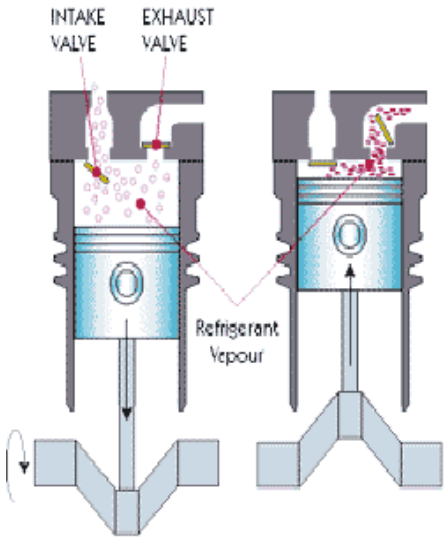

Figure 1.1: Reciprocating compressor. (Siemens, 2008).

Figure 1.1 shows a reciprocating compressor. When the piston is pushed up, the volume containing the gas is reduced, thereby increasing the pressure of the gas. A rotary compressor works in a similar manner, by expanding and taking in gas, and thereafter reducing the volume and releasing the gas afterwards. On the other hand, centrifugal and axial compressors accelerate the gas to a high velocity, and then decelerate it to convert the kinetic energy to potential energy. In axial compressors the deceleration takes place in the stator blade passages, before the gas leaves the compressor in the axial direction. In centrifugal compressors, the deceleration happens in the diffuser, and the gas leaves the compressor in a direction perpendicular to the drive shaft. The compressor type studied in this project is the centrifugal compressor.

Figure 1.2 shows a centrifugal compressor with a horizontally split outer casing. The casing is the outer shell of the compressor, built to withstand the pressure inside. Because of their principle of operation, axial and centrifugal compressors are also known as turbo- or continuous flow compressors. Reciprocating, rotary and axial type compressors will not be further discussed in this report, but more information can be found in (Boyce, 2003) and (Bloch, 2006).

Compressors have a wide range of applications, which will be briefly described below. A gas turbine consists of a compressor, a combustion chamber and a turbine. The compressor delivers compressed fluid to the combustion chamber. The increase in temperature in the combustion chamber creates an expansion of the fluid over the turbine, creating useful power output. Gas turbines are used in aircraft and marine propulsions and in electricity production. In order to transport gas in pipelines, for example in the process industry, compressors are used to obtain the differential pressure required between the pipe inlet and outlet. These compressors often work with high flows and low pressure ratios. Compressors used for transportation can be driven by electrical motors or gas turbines. On an offshore platform, gas turbines can be used, since the gas is easily available. However, electrical motors are becoming more popular due to the faster acting motor response. If the electricity for the motor comes from renewable energy sources, an electrical motor will be more environmentally sound than a gas turbine. Compressors are also used to supercharge internal combustion engines. The power of the engine can be increased if the pressure of the air is increased before it enters the engine, as discussed in (Erickson, 2008).

There are several mathematical models for a centrifugal compressor. A model developed for axial compressors by (Greitzer, 1976) was later extended to handle centrifugal compressors as well. While there exists other basic compressor models, this model was the first one to incorporate the non-linear, large oscillations during a surge cycle. This model was later modified to incorporate centrifugal compressors operating at variable speeds and include another non-linear effect called *rotating stall*. (Gravdahl and Egeland, 1999) developed a model based on the modified model of (Greitzer, 1976). The main difference is that the latter model is more physically based. Actual design parameters of the compressor are incorporated in the model. In (Gravdahl et al., 2002) certain parts of the model are improved by removing some of the uncertain parameters.

Figure 1.2: Centrifugal compressor with horizontally split outer casing. (Siemens, 2008).

1.3 Centrifugal compressors

Centrifugal compressors work by accelerating the fluid to a high velocity and then decelerate it in order to convert the kinetic energy of the gas to potential energy. Figure 1.3 shows the main parts of a centrifugal compressor. The main parts of a centrifugal compressor are the impeller, the diffuser and the collector/volute. The fluid enters the compressor axially with respect to the drive shaft. The doubly curved impeller blades are connected to the drive shaft, which rotates the impeller at a high speed. The impeller blades will increase the fluid's velocity. The static pressure of the fluid is increased when traveling from the inducer in the center of the impeller to the impeller tip. The inducer is sometimes referred to as the impeller eye. The fluid will then enter a diffuser, where the velocity is decreased. This will further increase the static pressure of the fluid. There are two main types of diffusers, vaneless and vaned diffusers. Vaned diffusers create separated divergent passages for the fluid. They take less space, but are more expensive than vaneless diffusers. Vaneless diffusers are also known as annular diffusers. They are larger, but cheaper to produce and give the compressor a larger operating range than a vaned diffuser. When the fluid exits the diffuser it is collected by the volute and led to the compressor outlet. In some

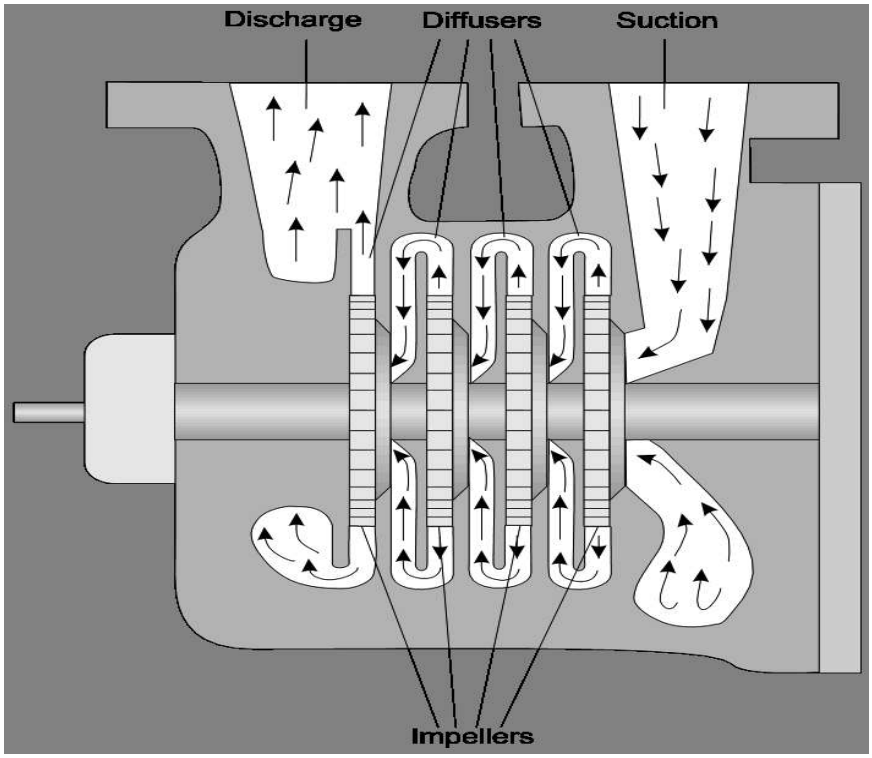

Figure 1.3: Internal view of a centrifugal compressor with four stages. (Siemens, 2008).

compressors the volute is also used as a diffuser. Centrifugal compressors do normally have more than one impeller and diffuser. They are called multi-stage compressors, different from single-stage compressors. A multi-stage compressor can be viewed as a series of single-stage compressors connected to the same drive shaft. Figure 1.3 shows a compressor with four stages, there are four impellers and diffusers in series. The gain of a multi-stage compressor will be illustrated with an example from (Asheim and Hvidsten, 1991). Consider the process of increasing the pressure P_1 of a fluid to a pressure P_2. A possibility is an adiabatic compression directly from P_1 to P_2. An adiabatic process is a thermodynamic process where no heat is transferred to or from the working fluid. Instead, consider the possibility of increasing the pressure over 2 stages. The optimization problem can be formulated, as shown in Equation 1.1:

$$W = W_1 + W_2 = RT_1 \frac{k}{k-1}\left[\left(\frac{P_2}{P_1}\right)^{\frac{k-1}{k}} - 1\right] + RT_2 \frac{k}{k-1}\left[\left(\frac{P_3}{P_2}\right)^{\frac{k-1}{k}} - 1\right] \quad (1.1)$$

W, W_1 and W_2 are the required work for compression, P_1 and T_1 are known inlet pressure and temperature. P_2 and T_2 are unknown pressure and temperature in the

intermediate stage. P_3 is the known outlet pressure. By differentiating Equation 1.1 with respect to P_2, and setting the resulting equation equal to zero, the optimization problem can be formulated, as shown in Equation 1.2:

$$opt.P_2 = \left(\frac{T_2}{T_1}\right)^{\frac{k}{2k-2}} \sqrt{P_3 - P_1} \tag{1.2}$$

Equation 1.2 can be further simplified if it is assumed that the gas is cooled to the inlet temperature between the stages, meaning that T_2=T_1. Equation 1.3 is a common equation used for calculating the multistage ratio:

$$opt.P_2 = \sqrt{P_3 P_1} \rightarrow \frac{P_2}{P_1} = \frac{P_3}{P_2} = r \tag{1.3}$$

where r is the constant optimal stage ratio. The value of r is normally chosen to be in the range of 4 to 6. Lower values of r will lead to a more complex process, while higher values increases the energy consumption of the process.(Bloch, 2006) presents an equation for multistage compressors, see Equation 1.4:

$$r_s = \sqrt[s]{r_t} \tag{1.4}$$

where r_s is the compression ratio per stage, s is the number of stages and r_t is the overall compression ratio. Industrial centrifugal compressors can have up to nine stages. Equation 1.4 is an approximation used for design purposes, because compression ratio per stage in a multistage compressor seldom is equal.

1.4 Compressor surge

Surge is a limit cycle oscillation in the compressor characteristics. Surge is a one-dimensional system instability, which only occurs in compressible flow systems (van Helvoirt, 2007).

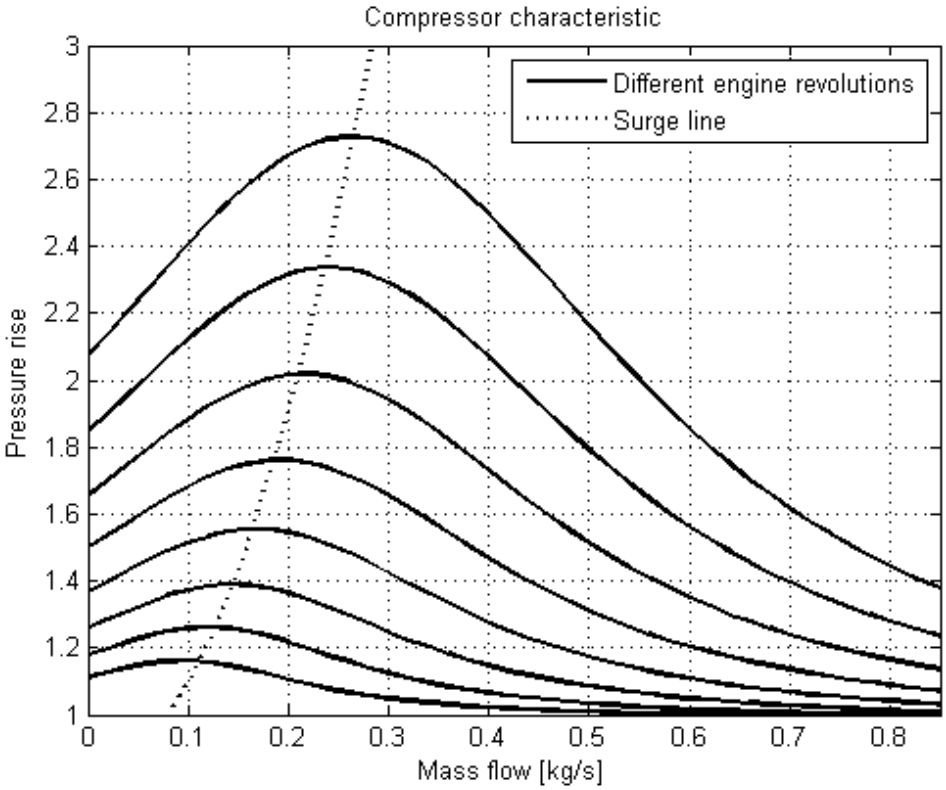

Figure 1.4: Compressor characteristics with surge line.

An example of a compressor characteristic curve, also called a compressor map, is given in Figure 1.4. The figure shows that the surge line for a compressor coincides with the peak of the characteristic curve for a given engine revolution. The stable region is to the right of the surge line, while the unstable region is on the left-hand side. If the mass flow through the compressor drops below the surge line, the compressor enters the unstable region, in which surge can occur. During a surge cycle, large variations in pressure and mass flow can occur. In (de Jager, 1995) four types of surge are defined, based on amplitude and frequency variations of the oscillations, namely mild surge, classic surge, deep surge and modified surge. Deep surge is the most severe of these types, as reversed mass flow can occur in the compressor. Figure 1.5 shows an example of the pressure and flow oscillations related to a deep surge cycle.

The flow reversal during deep surge can be very damaging for the compressor system, and the large vibrations following the surge can also damage other equipment. There are several unexpected events that can make the compressor enter surge. Changes in the production rate, pressure rise or flow rate demand can trigger surge

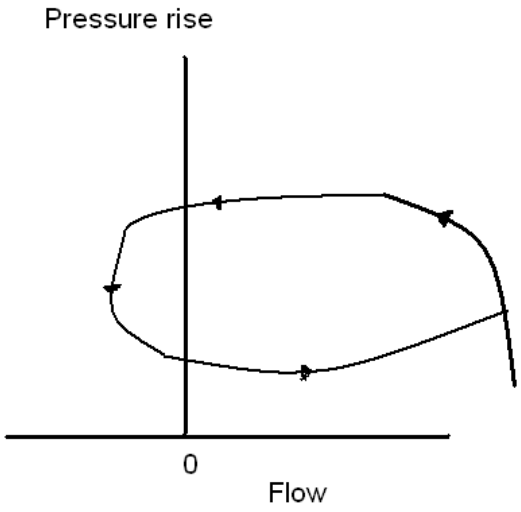

Figure 1.5: A typical deep surge cycle.

when the compressor adjusts its rotor speed to meet the new requirements. During a deceleration of the compressor, the pressure will drop slower than the mass flow, and this will drive the compressor towards the surge line, as can be seen in Figure 1.4. Another event that can trigger surge is significant changes in the gas composition. This can happen in an offshore oil and gas processing system. As shown in (Grong and Kylling, 2008), changes in the gas composition can move the surge line for the compressor, and cause the compressor to enter surge since mass flow and pressure remain the same. (Boyce, 2003) sums up the reasons that can lead to surge:

- Poor matching of the compressor to the system's requirements.
- Inappropriate compressor design.
- Inadequate antisurge control system.
- Unfavorable arrangement of piping and process components of the system, which often can magnify surge.

Surge is not the only effect that can change the performance of a centrifugal compressor. *Rotating stall* is an instability that causes a distortion in the circumferential flow through the compressor. One or more *stall cells* can travel around the circumference of the compressor. In the stall cells, flow is reduced or completely blocked.

Rotating stall causes the outlet pressure to drop, and causes vibrations in the impeller blades because the stall cells rotate at a speed of about 10-90 % of the rotor speed. Rotating stall can occur in centrifugal compressors, but is more important when considering axial compressors.

Choking is an effect that can occur when the flow reaches sonic velocity at a cross-section area of the compressor system. Choking sets the upper limit for the mass flow that the impeller can handle. If the ratio between the relative inlet gas velocity and the sonic velocity of the gas is equal to unity, choking occurs. Choking is also known as *stone wall*.

1.5 Active surge control

The possible damaging effects that compressor surge can lead to implies that this is a phenomenon one would like to avoid. Several methods for surge avoidance exist. The most widely used method in industrial compressor systems today is to use a recycle valve to divert gas from the compressor outlet and back to the inlet. This is to keep the flow through the compressor above the critical limit. For safety, a surge control line is chosen, normally about 10% to the right of the surge line defined by the compressor characteristics. A certain safety margin is needed because sudden changes in the system parameters can make the compressor entering surge. The major drawback of the recycle valve is that the gas is run through the same compressor several times. This increases the energy consumption of the compressor. This solution has proved reliable, but is somewhat inefficient.

An important addition to a recycle valve antisurge controller is the possibility for loop decoupling when there are multiple compressors in the system. If the first compressor in the chain approaches the surge area, and the antisurge controller opens the recycle valve, the mass flow upstream will drop. A production controller, monitoring the overall mass flow will, in turn, increase the mass flow within the system, thereby causing the antisurge controller to close the recycle valve. This leads to unnecessary oscillations in the mass flow of the system, and decreases the stability of the system. By letting the different controllers monitor and compensate each others actions, this can be avoided. Antisurge controller requirements are further discussed in (Bloch, 2006).

Surge avoidance and detection methods attempt to use measurements in order to detect incipient surge, and use a surge controller to prevent the compressor entering

full surge. A fast acting control system and fast actuators are needed for a successful result. This is a problem, and the reason for the very limited use of this solution.

Active surge control is a popular research field. The purpose of active surge control is to stabilize the compressor when operating within the unstable region of the compressor map. This is achieved by extending the stable operating envelope of the compressor. Modifications of the compressor or the controller must be done in order to be able to achieve this. Moving plenum wall, throttle valves, air actuators, close coupled valve, variable inlet guide vanes or drive torque control are examples of active surge schemes. (Grong and Kylling, 2008), (van Helvoirt, 2007) and (Gravdahl and Egeland, 1999) cover close coupled valves, while (Gravdahl et al., 2002) and (Bøhagen, 2007) use drive torque actuation for active surge control. Active surge control using drive torque is covered by an ABB patent, see (ABB Research Ltd, 2000). Despite the extensive research, an active surge control system has yet to become as popular as recycle valves in industrial compressor systems. This is mainly because of the need for rapid actuation when the compressor approaches the unstable region. In this thesis two solutions for active surge controllers will be studied in detail.

Chapter 2

Modeling of compressor characteristics

When a compressor is delivered from the manufacturer, system documentation is also supplied. One of the most important graphs is the *compressor characteristics*, also known as the compressor map.

Figure 2.1 shows an example of a compressor characteristic. This particular compressor is the one studied in (Gravdahl and Egeland, 1999) and (Bøhagen, 2007). Because the data for this compressor are particularly well documented, at the same time as it is currently placed in the basement of the Department of Engineering Cybernetics at NTNU, this compressor is chosen for the present studies. The solid lines in Figure 2.1 represent different engine revolutions (rpm). The revolutions range from 55000 rpm down to 20000 rpm. The x-axis represents the flow of gas. In this example mass flow($\frac{kg}{s}$) is used, while volume flow($\frac{m^3}{s}$) also can be used. Mass flow is mostly used in research based work on compressor control, while volume flow is widely used in industrial gas processing systems. The reason for this is that in order to know the mass flow, one must also know the molar density of the gas composition. Since the ratio of the different gas components can vary greatly and is difficult to measure efficiently, volume flow is easier to utilize. Along the y-axis of Figure 2.1, the pressure ratio is shown. The pressure ratio is the compressor outlet pressure divided by the inlet pressure, and represents the pressure rise in the compressor. The information from the compressor characteristics shows how the compressor will operate when the gas flow and the engine revolutions vary. Exact control of the gas flow can be difficult, especially on an oil platform where the operating conditions can vary. Controlling the engine revolutions is a normal way of controlling the compressor performance. However, some compressors operate at fixed revolutions, for example the compressor on the Snorre A platform studied in (Grong and Kylling, 2008). But the compressor characteristics give valuable information about the operating range of the compressor.

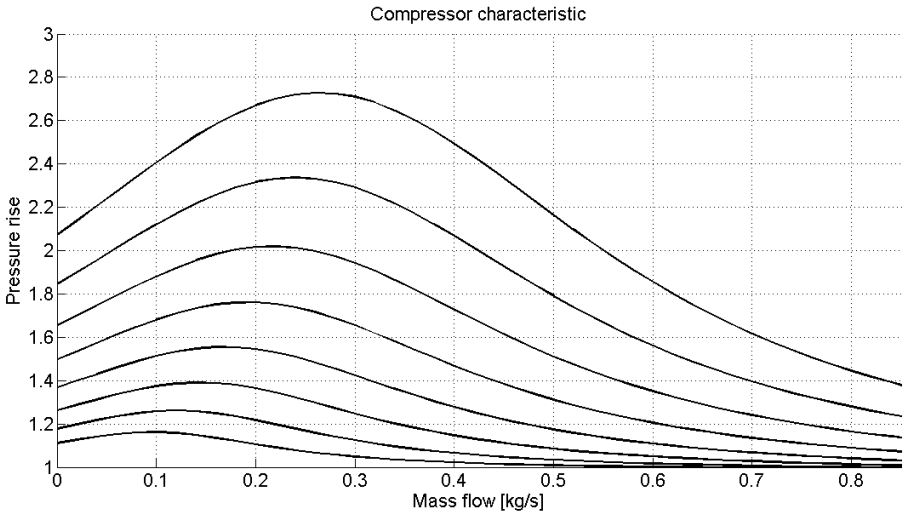

Figure 2.1: Compressor characteristics.

Information about point of surge and chocking can also be found in the compressor characteristics provided by the manufacturer.

On an offshore platform, it is important for the overall control system to know the state of the system. Regarding compressors, a better picture of their state of operation can be obtained by combining measurements from the compressor system with information from the compressor characteristics. The compressors on the Snorre A platform studied by (Grong and Kylling, 2008) and (Grong, 2008) were operating more or less at stationary points. This to ensure a stable gas-flow and pressure delivered to the customer.

For industrial systems, simplified models for the compressor characteristics have been developed and implemented. For example, a program testing these possibilities have been developed by (Neverlý et al., 2008). An example of a model of a compressor, based on inputs from the supplied compressor characteristic graphs, is the ConSi surge control package. For testing purposes, one can select points from the graphs and feed them into the program, which then provides an approximation of the complete compressor characteristics. The type of approximation used in this program is not known, as this is a business secret of Sicom Norge. However, the user instructions for the system can be found in (Siemens, 2000). Still, there is a great industrial need for easy-to-use and fast-acting compressor models based on actual compressor data.

2.1 Physical-based compressor model

The first model reviewed in this thesis is based on a physical model of the centrifugal compressor described by (Gravdahl and Egeland, 1999). This model is also used in (Grong, 2008). The model relies on the physical design parameters of the compressor to capture the behavior of the system.

In the following the constitutive equations for the physical-based model for the compressor characteristics will be presented. Figure 1.3 shows a sketch of the main parts of a centrifugal compressor. The average diameter D_1 of the inducer is given by the relationship:

$$D_1^2 = \frac{1}{2}(D_{l1}^2 + D_{h1}^2) \tag{2.1}$$

where D_{l1} is the diameter at inducer tip and D_{h1} is the diameter at the hub casing.

During operation, slip is an effect that will occur between the gas and the impeller blades. The slip makes the gas leave the impeller with a velocity less than the velocity of the impeller tip. Ideally, the gas would have the same velocity as the impeller. The slip factor is defined as:

$$\sigma \triangleq \frac{C_{\theta 2}}{U_2} \tag{2.2}$$

where σ is the slip factor, $C_{\theta 2}$ is the gas velocity at impeller tip and U_2 is the velocity of the impeller tip. Because the parameter $C_{\theta 2}$ is usually not known, other approximations exist, like the Stodola slip factor:

$$\sigma \approx 1 - \frac{\pi}{i} \frac{\sin(\beta_{2b})}{1 - \frac{C_{2a}}{U_2}\cot(\beta_{2b})} \tag{2.3}$$

where β_{2b} is the impeller backsweep angle, C_{2a} is the axial component of the gas velocity at the impeller tip and i is the number of impeller blades. The slip factor σ varies between 0 and 1. In (Gravdahl and Egeland, 1999) it is assumed constant, while in (Grong and Kylling, 2008) a variable slip factor σ is implemented using an approximation of C_{2a}. If the slip factor is assumed constant, the specific enthalpy without any losses delivered to the gas is given by the expression:

$$\Delta h_{0c,ideal} = \sigma U_2^2 \tag{2.4}$$

According to (Watson and Janota, 1982), (Ferguson, 1963) and (Nisenfeld, 1982) there are two types of major efficiency losses in centrifugal compressors, incidence

losses and fluid friction losses. Both types of losses occur in the impeller and the diffuser and can be expressed as:

$$\Delta h_{ii} = \frac{1}{2}\left(U_1 - \frac{\cot(\beta_{1b})m}{\rho_{01}A_i}\right)^2 \tag{2.5}$$

where Δh_{ii} is the incidence loss at the impeller, U_1 is the tangential velocity at the rotor, β_{1b} is the fixed impeller blade angle and ρ_{01} is the constant stagnation inlet density. Δh_{id} is the incidence loss at the diffuser and can be expressed as:

$$\begin{aligned} \alpha_{2b} &= \arctan\left(\frac{D_1\tan(\beta_{1b})}{\sigma D_2}\right) \\ \Delta h_{id} &= \frac{1}{2}\left(\frac{\sigma D_2 U_1}{D_1} - \frac{m\cdot(\alpha_{2b})}{\rho_{01}A_d}\right)^2 \end{aligned} \tag{2.6}$$

where D_2 is the impeller diameter at the tip and A_d is the cross section area of the diffuser.

Moreover, the fluid friction loss at the impeller, Δh_{fi} is given as:

$$\begin{aligned} \Delta h_{fi} &= \frac{C_h l}{2D\rho_{01}^2 A_1^2 \sin^2(\beta_{1b})} m_2 = k_{fi} m^2 \\ f &= 0.3164(Re)^{-0.25} \\ C_h &= 4f \end{aligned} \tag{2.7}$$

where Re is the fluid Reynolds number, f is the friction factor, C_h is the surface friction loss coefficient. Equation 2.7 is the frictional loss of a mass flow passing through a pipe with mean hydraulic diameter D. Δh_{fd} can be modeled in the same way by using k_{fd} in Equation 2.7. There are also other minor losses that occur in centrifugal compressors. Clearance, back-flow, volute and diffusion losses are incorporated into a single constant loss in the model, and assumed to be less than 10%. These losses are denoted Δn. (Pampreen, 1973), (Watson and Janota, 1982), (Cumpsty, 1989) and (Erickson, 2008) have further information about compressor losses.

By combining Equation 2.4, Equation 2.5, Equation 2.6 and Equation 2.7 for both impeller and diffuser, one obtain the equations for the isentropic efficiency for the compressor.

$$\begin{aligned} \eta_i(m, U_1) &= \frac{\Delta h_{0c,ideal}}{\Delta h_{0c,ideal} + \Delta h_{loss}} - \Delta n \\ \Delta h_{loss} &= \Delta h_{fi} + \Delta h_{ii} + \Delta h_{fd} + \Delta h_{id} \end{aligned} \tag{2.8}$$

An isentropic process in thermodynamics is one where the entropy remains constant in the working fluid. Because heat is transferred to the gas, the temperature of the gas increases. To maintain constant entropy, cooling of the fluid is needed to keep the process isentropic. Compression of gas is more accurately modeled as a polytropic process. The thermodynamics for compression of gas are elaborated in Appendix B, while further details about fluid dynamics can be found in Appendix C.

The outlet pressure p_2 for forward flow can be formulated as:

$$p_2 = \left(1 + \frac{\eta_i(m, U_1)\Delta h_{0c,ideal}}{T_{01}C_p}\right)^{\frac{k}{k-1}} p_{01} = \Psi_c(U_1, m)p_{01} \forall m > 0 \tag{2.9}$$

where Ψ_c is the compressor characteristics. The complete deduction of Equation 2.9 can be found in Appendix B. Because of compressor surge, being discussed previously, the model must be augmented. To be able to model negative mass flow (i.e. reversed flow), which can happen during surge, the characteristics must be modified as:

$$\Psi_c(U_1, m) = \begin{Bmatrix} c_n m^2 + \Psi_{c0}(U_1) & , & m \leq 0 \\ \left(1 + \frac{\eta_i(m,U_1)\Delta h_{0c,ideal}}{T_{01}C_p}\right)^{\frac{k}{k-1}} & , & m > 0 \end{Bmatrix} \tag{2.10}$$

where Ψ_{c0} is the compressor shut off valve and c_n is a constant scaling factor. A choice regarding Ψ_{c0} in order to make $\Psi_c(U_1, m)$ continuous in m, is shown in Equation 2.11:

$$\Psi_{c0}(U_1) = \left(1 + \frac{\eta_i(m, U_1)\Delta h_{0c,ideal}}{T_{01}C_p}\right)^{\frac{k}{k-1}} \Bigg|_{m=0} \tag{2.11}$$

2.2 Polynomial approximation method

Another common approach for approximating compressor characteristics is to use a polynomial approximation. (Moore and Greitzer, 1986) use a 4^{th} order polynomial

to describe the compressor characteristic Ψ_c. This is the preferred method in most compressor modeling. Figure 2.2 shows an example of a 4^{th}-order approximation of a single speed line for an industrial compressor stationed on the Snorre A platform. The circles are data points from the manual provided by the compressor manufacturer, and the solid line is the 4^{th}-order approximation, found by using the *polyfit*-function in MATLAB.

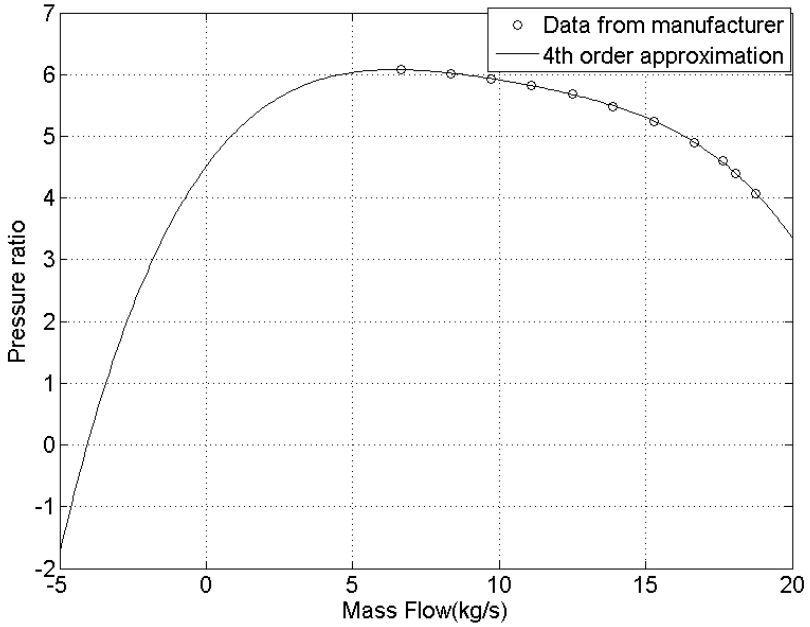

Figure 2.2: Example of 4^{th}-order approximation of compressor characteristics.

The method chosen for calculating a 4^{th}-order polynomial in this thesis is the same as the one used in (van Helvoirt, 2007). The approximation was carried out in full dimension, and scaled down afterwards.

$$\Psi_c(m,N) = \Psi_c(0,N) + V(N)\left[1 + \frac{3}{2}\left(\frac{m}{W(N)} - 1\right) - \frac{1}{2}\left(\frac{m}{W(N)} - 1\right)^3\right] \quad (2.12)$$

Equation 2.12 is the full dimension of the cubic polynomial used. N is the number of engine revolutions. Figure 2.3 shows the definition of the parameters $\Psi_c(0)$, V and W related to the compressor characteristics. The choice to include N in the approximation gives increased accuracy, but increases the complexity of the calculations as well. The cubic polynomial in Equation 2.12 can be rewritten as:

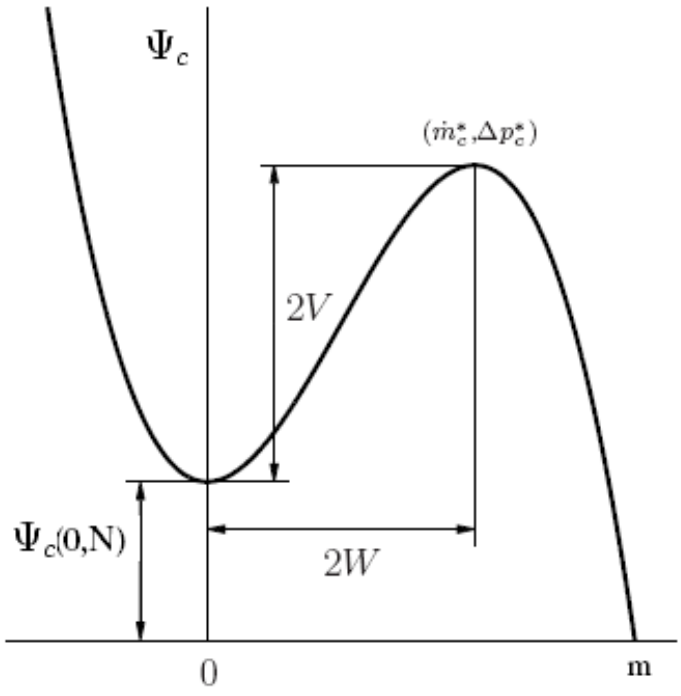

Figure 2.3: Definition of the parameters entering the cubic polynomial. Based on ideas from (van Helvoirt, 2007).

$$\Psi_p(m, N) = a_0(N) + a_2(N)m^2 + a_3(N)m^3 \tag{2.13}$$

This form of the cubic polynomial is used in several research papers, such as (Willems, 2000), (Bøhagen, 2007), (van Helvoirt, 2007) and (Grong and Kylling, 2008) and is also described in (Gravdahl and Egeland, 2002).

Figure 2.3 shows the definition of the parameters ΔP_c, V and W in Equation 2.12. The coefficients a_0, a_2 and a_3 are chosen such that:

$$
\begin{aligned}
a_0 &= \Psi_c(0) \\
a_2 &= \frac{3V(N)}{2W^2(N)} \\
a_3 &= \frac{-V(N)}{2W^3(N)}
\end{aligned}
\tag{2.14}
$$

Based on these definitions of the coefficients, the parameters are fitted to the speed lines of the compressor characteristic shown in Figure 2.1 in a least square way. In practice, it is impossible to obtain stable measurements for the compressor when operating within the unstable region of the compressor characteristic (i.e. to the left of the point of surge). At the same time the different speed lines must not cross each other in the model. Therefore, the speed lines must be extended. Based on this approach, (Bøhagen, 2007) and (van Helvoirt, 2007) construct a new approximation for the unstable region when the mass flow is negative, which means flow reversal in the compressor:

$$\Psi_c(m, N) = a_4(N)m^2 + a_5(N), m < 0 \tag{2.15}$$

The parameter $a_5(N)$ in Equation 2.15 is the compressor characteristics at zero mass flow for a specified rotational engine speed. Given this extension, Equation 2.13 and Equation 2.15 can be combined to form a complete and continuous approximation of the compressor characteristics.

2.3 Table lookup method

Another approach for modeling compressor characteristics is used in (Kylling, 2008). When trying to fit a polynomial approximation to the compressor characteristic of a multi-stage industrial compressor, it was observed that the fit was inadequate. Therefore, a lookup-table was suggested as a better solution. The method for calculating additional speed-lines, lying between the given speed-lines from the manufacturer, is as follows(from (Kylling, 2008)).

Figure 2.4 explains the notation used in the procedure described below. The rotational speed in a given point $[x_2, y_2]$ of the compressor characteristics can be found by:

- Calculating the shortest distance from the known lower speed-line ($Pr_{\omega=1}(m)$) to the speed-line lying above ($Pr_{\omega=2}(m)$) passing through the point $[x_2, y_2]$.

- $[x_1, y_1]$ is the point that the straight line found in the previous point intersects the lower speed-line, while $[x_3, y_3]$ is where the line intersects the upper speed-line.

- The distance from $[x_2, y_2]$ to $[x_1, y_1]$ can be calculated as:

$$L_1 = \sqrt{(x_1 - x_2)^2 + (y_1 - y_2)^2} \tag{2.16}$$

- The distance from $[x_2, y_2]$ to $[x_3, y_3]$ can be calculated as:

$$L_2 = \sqrt{(x_3 - x_2)^2 + (y_3 - y_2)^2} \tag{2.17}$$

- The speed in the point $[x_2, y_2]$ can now be calculated as:

$$\omega_2 = \omega_1 + (\omega_3 - \omega_1) \cdot \frac{L_1}{L_1 + L_2} \tag{2.18}$$

- A decision must then be made of how many estimated speed-lines that are desired. In the following equation, the choice of nine is made. First, nine new points, denoted $[x_{ai}, y_{ai}]$ are calculated as:

$$\begin{aligned} x_{ai} &= x_1 + (x_3 - x_1)\frac{i}{10} \\ y_{ai} &= y_1 + (y_3 - y_1)\frac{i}{10} \end{aligned} \tag{2.19}$$

- Using the points found in Equation 2.19, the speed in these points can be calculated by:

$$\omega_{ai} = \omega_1 + (\omega_2 - \omega_1)\frac{i}{10} \tag{2.20}$$

The point $[x_2, y_2]$ must be carefully chosen such that it is guaranteed to lie between the speed-lines. This can be assured by selecting the point as:

$$\begin{aligned} x_2 &= m \\ y_2 &= 0.5Pr_1(m) + 0.5_h(m) \end{aligned} \tag{2.21}$$

This calculation is repeated for every available speed-line, thereby generating the estimated speed-lines $Pr_{\omega=ai}(m)$. The MATLAB function *interp1* with the method *spline* can be utilized to generate the new speed-lines ($Pr_{\omega=0.9+0.005i}(m)$).

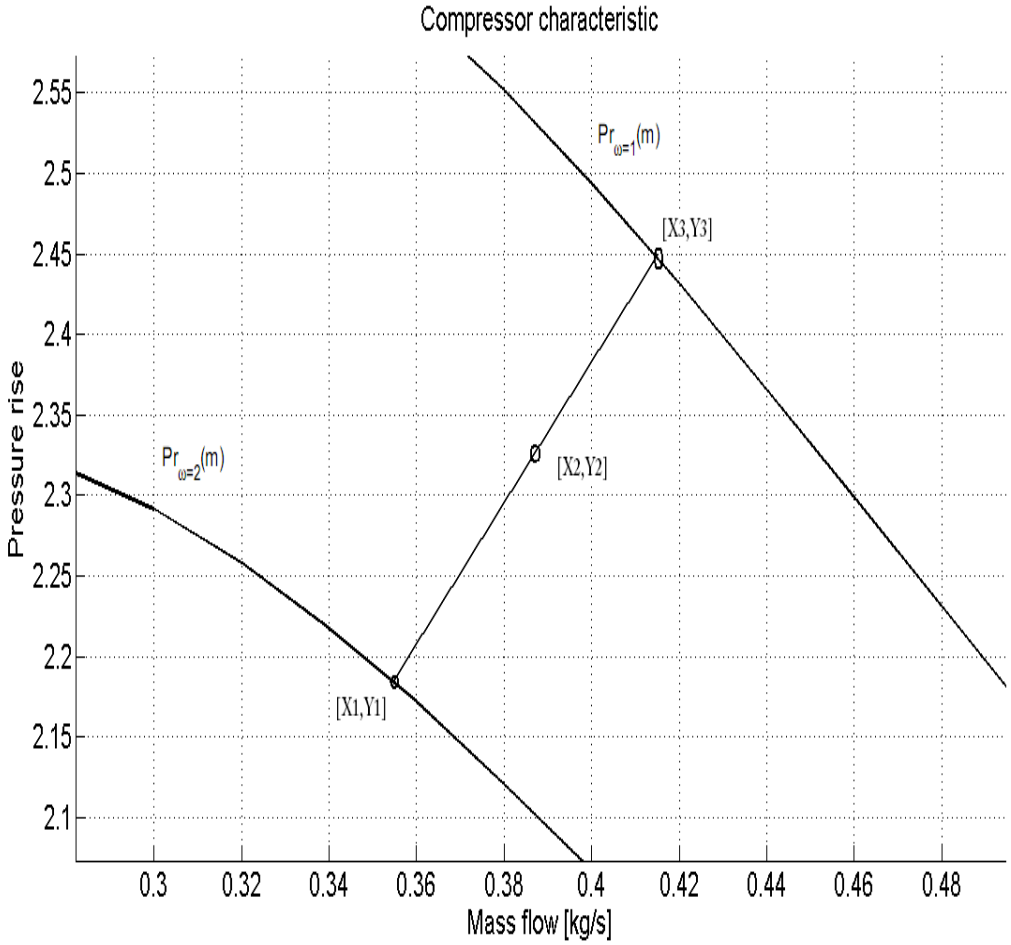

Figure 2.4: Notation used for estimation of new speed lines. Based on data from (Kylling, 2008).

2.4 Performance testing

In this section the three different solutions used for modeling the compressor characteristics is implemented in MATLAB and tested with respect to run-time. They are all implemented in a matlab-script, and a second script executes the first script several times, until the complete set of the compressor characteristics is found. The MATLAB-functions *tic* and *toc* are used to check execution time. MATLAB is restarted before each test. In order to arrive at a conclusion on which solution that has the lowest run-time and the least hardware demand, the test is carried out on two different computer systems. The specifications of the first system are:

- Intel Core 2 Quad Q6600 2.4GHz
- Corsair TWIN2X 6400C4 DDR2 RAM, 4096MB CL4
- MS Win Vista Home Premium English
- MATLAB R2007b

The specifications of the second system are:

- Intel Centrino 2.0GHz
- 1024MB RAM
- Windows XP PRO OEM Norsk
- MATLAB R2007b

The equations describing the compressor characteristic in the first model, found in Equation 2.10, are implemented in SIMULINK, as shown in Figure 2.5.

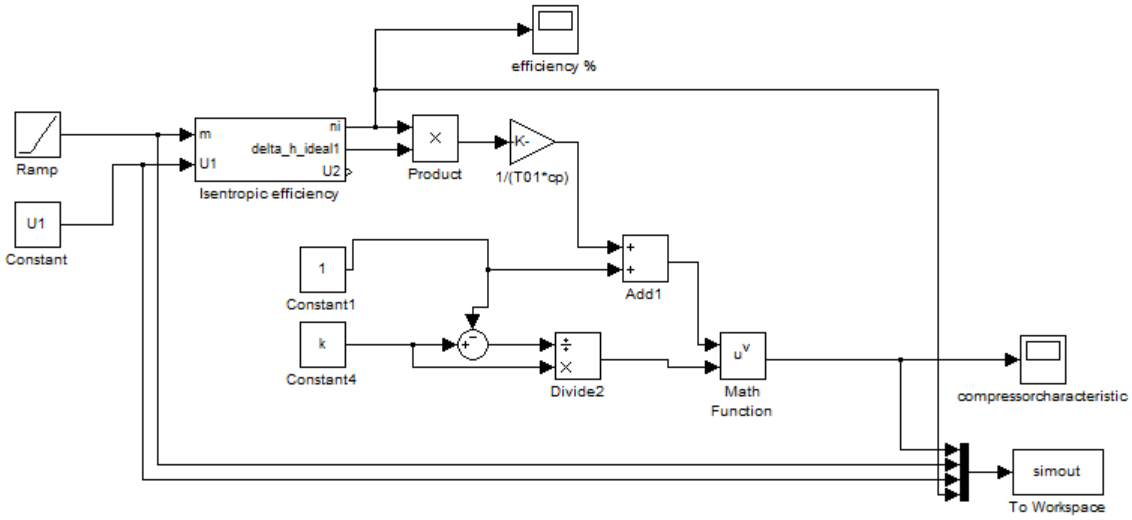

Figure 2.5: Physical model of compressor characteristics implemented in SIMULINK.

The ramp-function is used to generate the range of mass flow in the simulation. For each required speed-line, the model is run and the results stored. When all the different speed-lines have been found, the final result is presented in a graph. For timing the simulations, the scopes in Figure 2.5 are removed to increase performance.

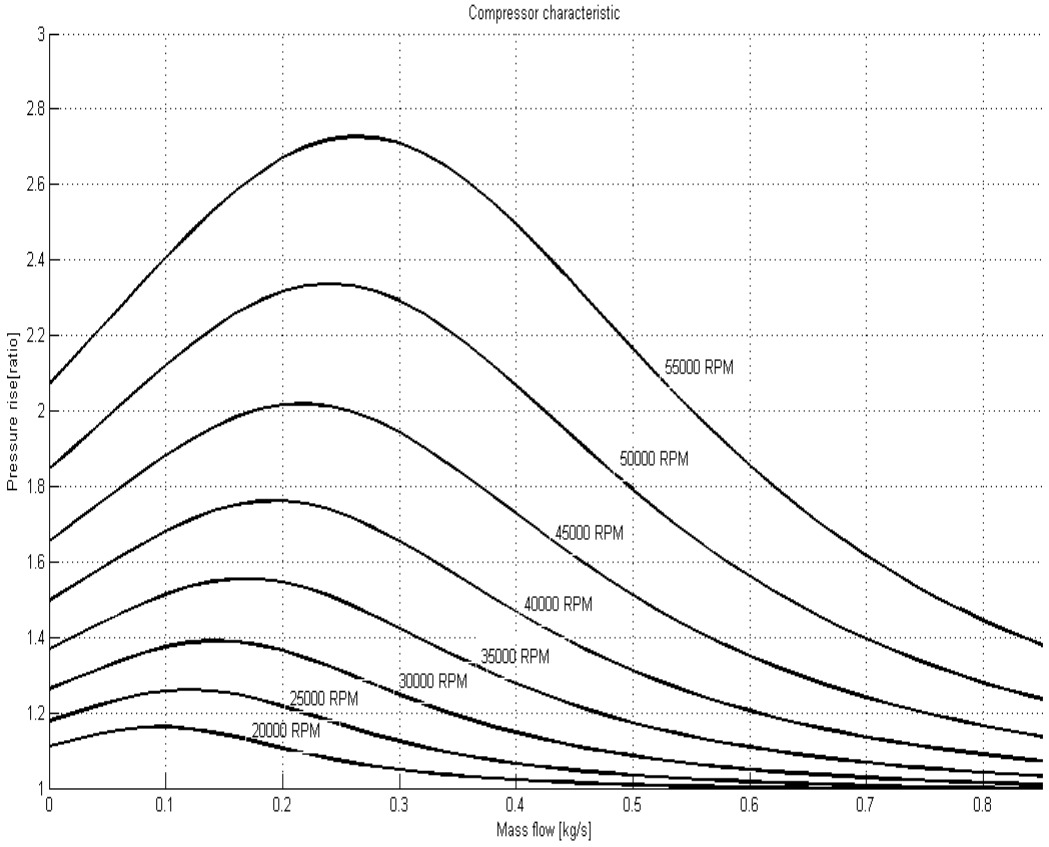

Figure 2.6: Compressor characteristics for physical model of compressor.

A scope will increase the time required to simulate a system because of the extra simulation outputs, but by just processing the data from the *to workspace*-block the simulation can be improved. The final result of the simulation is plotted in Figure 2.6

Figure 2.6 shows a good representation of the compressor characteristic with regard to the point of surge (peak of each speed-line), the compressor ratio and the mass flow range. This consistency is obtained because well documented data for the compressor have been used, taken from (Gravdahl and Egeland, 1999). This particular compressor is used for research and development at NTNU, and is therefore well documented.

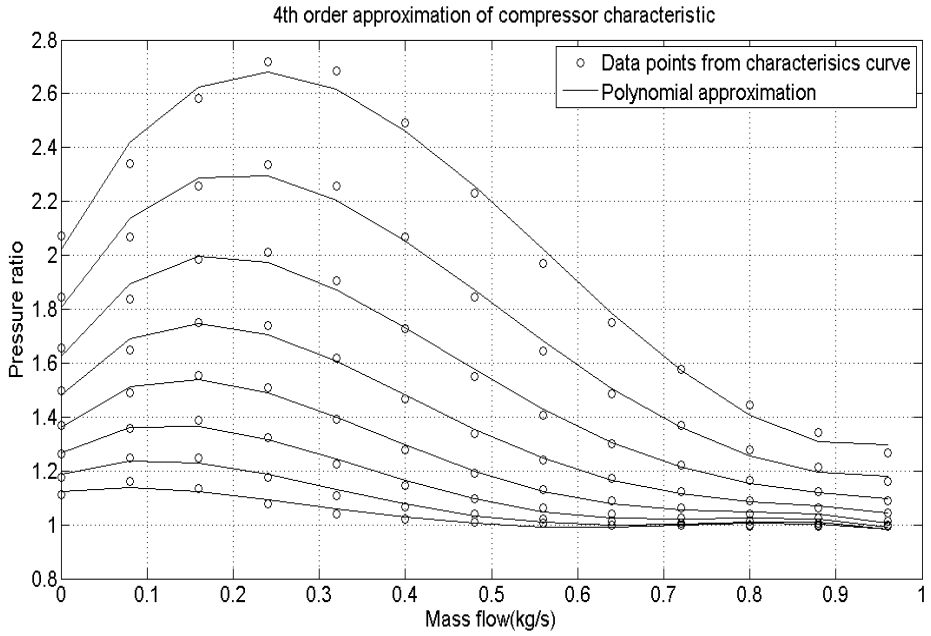

Figure 2.7: 4^{th}-order approximation of compressor characteristic.

Figure 2.7 shows the final result for the 4^{th}-order polynomial approximation of the compressor characteristic. The overall agreement is reasonable in the sense that the computed lines do not depart significantly from the measured data points. These calculations are carried out using only 10 points per speed-line. If a better fit is aimed at, more points can be extracted from the original compressor characteristics and used in the approximation.

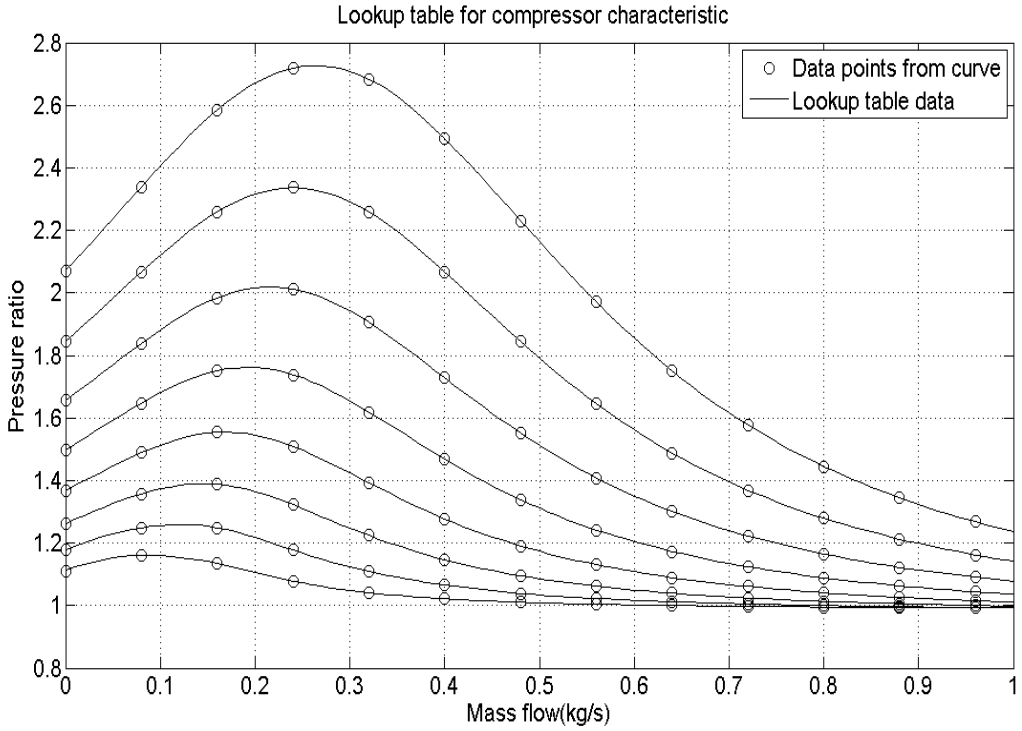

Figure 2.8: Table lookup method for compressor characteristics.

Figure 2.8 shows the final result for the lookup table approximation. The overall agreement between the data points and the curves is very good. The approximation follows the original data points almost exactly, and therefore is a good representation of the compressor characteristics. As for the 4^{th} order approximation, more points can be extracted from the original compressor characteristics and used in the approximation to obtain an even better fit.

Table 2.1: Results from tests of physical model on system 1.

Test	**Time**	**CPU**	**RAM**
1^{st}. run	$4.3511[s]$	23.0%	3.0%
2^{nd}. run	$4.4216[s]$	25.0%	3.0%
3^{rd}. run	$4.1191[s]$	25.0%	2.0%
Average	**4.2973**[s]	**24.3**%	**2.7**%

Table 2.2: Results from tests of physical model on system 2.

Test	**Time**	**CPU**	**RAM**
1. run	5.9454[s]	91.0%	3.9%
2. run	5.8300[s]	93.0%	3.8%
3. run	6.0009[s]	92.0%	3.9%
Average	**5.9254**[**s**]	**92.0**%	**3.9**%

Table 2.3: Results from tests of 4^{th}-order approximation on system 1.

Test	**Time**	**CPU**	**RAM**
1. run	0.7412[s]	21.0%	1.0%
2. run	0.8722[s]	17.0%	1.0%
3. run	0.9149[s]	17.0%	1.0%
Average	**0.8428**[**s**]	**18.3**%	**1.0**%

Table 2.4: Results from tests of 4^{th}-order approximation on system 2.

Test	**Time**	**CPU**	**RAM**
1. run	1.1366[s]	67.0%	0.59%
2. run	1.1312[s]	72.0%	0.59%
3. run	1.0835[s]	57.0%	0.59%
Average	**1.1171**[**s**]	**65.3**%	**0.59**%

Table 2.5: Results from tests of table lookup method on system 1.

Test	**Time**	**CPU**	**RAM**
1. run	32.5539[s]	27.0%	0.5%
2. run	27.0768[s]	39.0%	1.0%
3. run	26.3537[s]	33.0%	1.0%
Average	**28.6615**[**s**]	**33.0**%	**0.8**%

Table 2.6: Results from tests of table lookup method on system 2.

Test	**Time**	**CPU**	**RAM**
1. run	46.8987[s]	100.0%	1.3%
2. run	45.2755[s]	100.0%	1.4%
3. run	46.6758[s]	100.0%	1.3%
Average	**46.2833**[**s**]	**100.0**%	**1.3**%

Tables 2.1-2.6 show the results of the tests carried out on the two different computer systems. CUP- and RAM usage are listed as percent of the total CPU and RAM for the two different computer systems.

2.5 Evaluation

There are several important criteria for evaluating the different models for compressor characteristics.

- Simulation runtime
- Accuracy
- Scope of use
- Ease of implementation

The simulation runtime is the main parameter that has been tested in the previous section, and gives an indication of the efficiency of the different models. The accuracy of the characteristics is important, specially with regard to the point of surge. If the models are used for research purposes, accuracy is often the overriding concern. In addition, the scope of use for the model is important, because a model used for software-testing, production optimization simulations or scientific research does not have the same requirements. In this thesis, the main focus is on a model which can compete with the one currently used for testing the recycle valve controller from ConSi Maps, see (Siemens, 2000). Hence, the accuracy in the unstable region is less important, while the point of surge is very important when evaluating the recycle valve controller. Also, model implementation is important.

Tables 2.1-2.6 show the results of the performance tests of each of the different models carried out on the two different computer systems. The first noticeable difference is the simulation time for the table lookup method compared to the other two. It is about 29 seconds for the first system and 46 seconds for the second one, compared to 0.8 and 1.1 seconds for the 4^{th}-order polynomial method. This is because the method for the table lookup, as described above, is time-consuming when additional speed-lines are generated. Each new line requires that the points needed for the calculations must be found. Subsequently, calculations for each single point must be carried out. This takes significantly longer time than the other two methods. The physical model is somewhat slower than the 4^{th}-order method, with 4 and 6 seconds for the physical model compared to 0.8 and 1.1 seconds for the polynomial method. This is because of the additional calculations needed for the physical method based

on Equation 2.10, while the calculations for the 4^{th}-order method is very fast (provided that all information needed according to Figure 2.3 is available). And when the polynomial is found, the calculations required to obtain the additional speed-lines are straightforward. None of the methods demand much RAM. The physical model needs the most, since there is a lot of intermediate calculations that must be saved in the memory. The table lookup method is the most CPU-consuming method, considering all the work required to trace the given lines and calculate new ones. Because of the age of the second computer system, which is five years, some of the results obtained in those tests would probably improve with new hardware. But the main conclusion for this test is that the table lookup method is more time-consuming than the other two.

Each of the different models have requirements regarding how easy they are to implement. In this thesis, two of the models require that several data points are collected from the compressor characteristic provided by the manufacturer. Both the polynomial method and the table lookup method try to fit the approximations to the data points. This is opposed to the physical model, where all of the required parameters for this particular compressor are known. However, the latter is rarely the case for most compressors. Therefore, another approach must be used to obtain the missing parameters. This can be done by using an optimization algorithm to fit the characteristics from Equation 2.10. This method is used and described in (Grong and Kylling, 2008) and (Grong, 2008). According to these references, a problem can be that the numerical parameters either become too large or too small compared to the real values of the compressor. This is specially the case when the optimization algorithm tries to fit the parameters of a single stage model to data from a multistage compressor. A multistage model would require coupling of single stage models in series, thereby increasing the complexity and run-time. Therefore, multistage compressors are normally simulated as single-stage compressors. In comparison, the 4^{th}-order method and the table lookup method can represent a multistage compressor directly from the compressor characteristics given by the manufacturer. But the need for parameter estimation for the physical model makes this approach more complex than that required for the polynomial method and the table lookup method. The physical model will also loose some of its physical relevance, since the parameters can attain values that deviate strongly from the actual values of the compressor.

Although the table lookup method is slow, it has some advantages. If all calculations needed can be carried out beforehand, the method is very useful to simulate compressor characteristics. And if the initial calculations are done, the table lookup itself is very quick. This means that the long simulation times reported in Table 2.5 and Table 2.6 do not mean that the lookup table method is useless compared to the

other two.

Based on the above simulations and considerations some conclusions can be drawn. It is clear that the physical representation of the compressor characteristic has a very limited use. This is because of the required information being needed for the model, which must be obtained either from data sheets or by parameter estimation based on the compressor characteristics supplied by the manufacturer. The performance of the physical model implemented in this thesis is good, but this is because the compressor is relatively small and is well documented. The physical model is best suited when used for research on specific parts of a compressor system, such as active surge controllers. The 4^{th}-order polynomial method is shown to be very easy to implement in a computer program, where the extracted points from the compressor characteristic are fed into an algorithm which then calculates the polynomials. It is reasonable to assume that the recycle valve controller test program from ConSi MAPS(Siemens, 2000) is based on a polynomial method. The short calculation time means that this solution can be useful in an online environment, where new compressor characteristics must be calculated fast due to rapid changes in the processing system. But the initial polynomials must be calculated beforehand. Also the table lookup method performs very well, but the initial calculations being needed to obtain the extra speed-lines are very time-consuming. This means that for an online system, all the required speed-lines must be known in advance, which is not always the case. However, many compressors operate at more or less stationary points in order to maintain the delivery conditions of the gas supply. For research applications, it is a great advantage that the table lookup method provides a very good representation for both single and multistage compressors. The time-consuming initial calculations are something that normally needs to be be done just once for a given compressor characteristic. This suggests that the table lookup method is a better solution for representing compressor characteristics in research based work, while the 4^{th}-order polynomial method will perform better in an online simulation environment.

2.6 Parameter identification for a compressor

Another approach for representing the compressor characteristics in a dynamic model is to use parameter identification. This is a relatively new field in compressor modeling, but there are indications that this can be a better alternative than the normal tuning of a compressor model. This approach is described in (van Helvoirt et al., 2005). In their paper, the Greitzer lumped parameter compressor model is used.

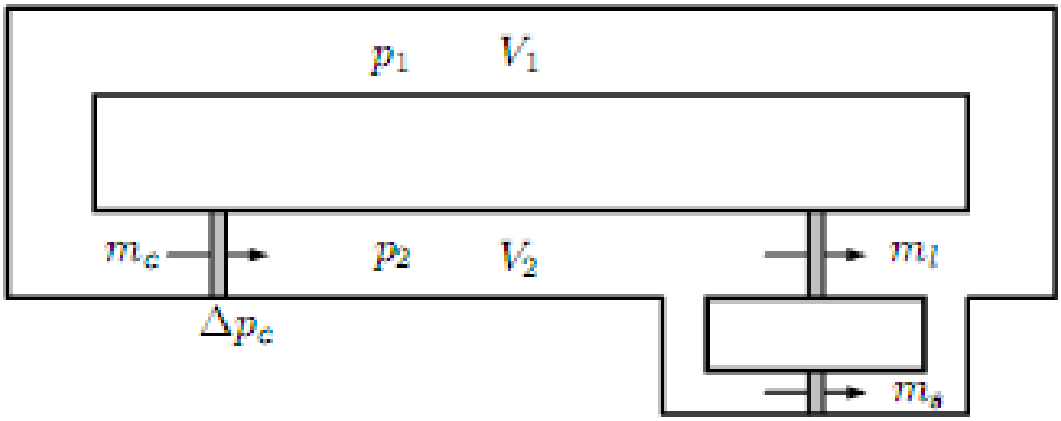

Figure 2.9: Greitzer lumped parameter model. From (van Helvoirt et al., 2005).

Based on Figure 2.9 the model can be formulated as:

$$\begin{aligned} \frac{dm_c}{dt} &= \alpha(\Delta p(m_c, N) - \Delta p) \\ \frac{d\Delta p}{dt} &= \beta(m_c - m_l(\Delta p, u_1) - m_s(\Delta p, u_s)) \end{aligned} \tag{2.22}$$

where $\Delta p = p_2 - p_1$, m_l is the outlet throttle valve and m_s the recycle valve. The parameters α and β are defined as:

$$\begin{aligned} \alpha &= \frac{A}{L} \\ \beta &= \frac{a_{01}^2}{V_1} + \frac{a_{01}^2}{V_2} \end{aligned} \tag{2.23}$$

An approximate realization algorithm is used to construct a Linear Time Invariant (LTI)-system based on step response data from the compressor system. This means that the step response data must be measured for the specific compressor system in question. For an offshore compressor system this could be done during maintenance shutdowns. Compressors are currently tested for surge during such shutdowns, where the mass flow through the compressor is brought down to the level where vibrations start to occur. Then it is assumed that the critical mass flow at the point of surge is somewhat lower than the measured mass flow. This means that also step response data can be extracted during these maintenance shutdowns. (van Helvoirt et al., 2005)

have shown that by constructing a first order LTI-system operating within the stable region of the compressor characteristic, two separate compressor model parameters can be determined independently. This implies that instead of having to measure or alternatively approximate the model parameters, like the values for A or L, they can be found by parameter identification. This can extend the use of the physical model for the compressor characteristics because the required system parameters then more readily can be determined. However, more work is needed before this method can compete with the other methods mentioned above.

Chapter 3

Close coupled valve

The use of a close coupled valve (CCV) was presented in (Gravdahl and Egeland, 1999). The approach is to introduce a valve close to the plenum volume in the compressor. Close coupled valve means that there is no mass storage of gas between the compressor outlet and the valve, as can be seen from Figure 3.1.

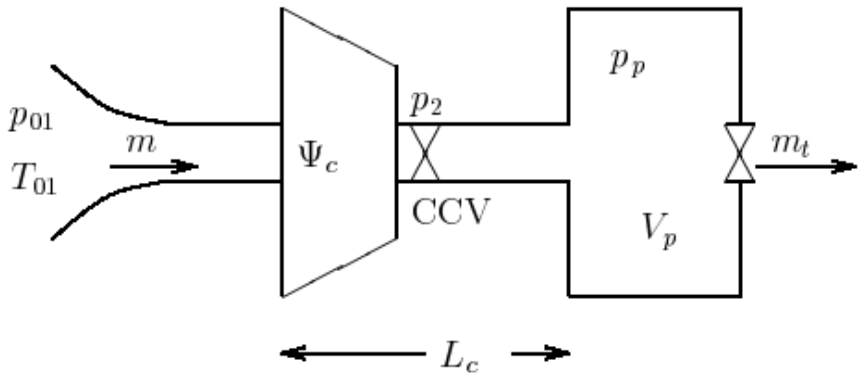

Figure 3.1: Compressor system with close coupled valve. From (Gravdahl and Egeland, 1999).

3.1 CCV control law

Based on the assumption that there is no mass storage of gas between the compressor outlet and the valve, the pressure increase in the compressor and the pressure drop across the valve can be combined into an *equivalent compressor*. This is needed in order enable the valve to control the characteristic of the equivalent compressor. This

is done according to Equation 3.1:

$$\Psi_e(m, U_1) = \Psi_c(m, U_1) - \Psi_v(m, U_1) \tag{3.1}$$

where Ψ_e is the characteristics of the equivalent compressor, and Ψ_v the characteristics of the CCV. To simulate the complete compressor system, equations for the pressure, mass flow and rotational speed of the drive shaft must be obtained. These equations will be the same as those used in (Grong, 2008). The outlet mass flow from the compressor is modeled as a mass flow trough a throttle valve, as given by Equation 3.2:

$$m_{out} = k_l \sqrt{p_p - p_{01}} \tag{3.2}$$

where k_l is the throttle gain, assumed to be proportional to the throttle opening.

The compressor torque τ_c can be modeled as follows:

$$\tau_c = |m| \frac{D_2}{2} \sigma U_2 \tag{3.3}$$

The complete model for the centrifugal compressor can now be formulated as:

$$\begin{aligned} \dot{p}_p &= \frac{a_{01}^2}{V_p}(m - k_l\sqrt{p_p - p_{01}}) \\ \dot{m} &= \frac{A}{L}\left((\Psi_c p_{01}) - p_p\right) \\ \dot{U}_1 &= \frac{D_1}{2I}(\tau_l - \tau_c) \end{aligned} \tag{3.4}$$

where a_{01} is the inlet stagnation sonic velocity, V_p is the plenum volume and Ψ_c is the compressor characteristics, as described by Equation 2.10. To be able to control the outlet pressure of the compressor, a pressure regulator will be added to the torque from the engine, τ_l. This is a simple PID-regulator, tuned roughly using the Ziegler-Nichols method. [p_0, m_0] are the equilibrium values for the intersection of pressure and mass flow in the compressor characteristics and U_d is the desired set-point for the rotor speed. First, some error variables must be defined:

$$\begin{aligned} \hat{p} &= p_p - p_0 \\ \hat{m} &= m - m_0 \\ \hat{U} &= U_1 - U_d \end{aligned} \tag{3.5}$$

The error variables in Equation 3.5 must be included in the dynamic equations given by Equation 3.4:

$$\begin{aligned}\hat{m}_{out}(\hat{p}) &= m_{out}(\hat{p} + p_0 - m_0)\\ \hat{\Psi}_c(\hat{m}, \hat{U}) &= \Psi_c(\hat{m} + m_0, \hat{U} + U_d) - p_0\\ \hat{\Psi}_v(\hat{m}, \hat{U}) &= \Psi_v(\hat{m} + m_0, \hat{U} + U_d) - p_0\end{aligned} \tag{3.6}$$

Equation 3.4 can now be rewritten using Equation 3.1 and Equation 3.6:

$$\begin{aligned}\dot{\hat{p}} &= \frac{a_{01}^2}{V_p}(\hat{m} - \hat{m}_{out}(\hat{p}))\\ \dot{\hat{m}} &= \frac{A}{L}((\hat{\Psi}_c(\hat{m}, \hat{U}) - \hat{\Psi}_v(\hat{m}, \hat{U}))p_{01} - \hat{p})\\ \dot{\hat{U}} &= \frac{D_1}{2I}(\hat{\tau}_l - \hat{\tau}_c)\end{aligned} \tag{3.7}$$

where $\hat{\tau}_l$ and $\hat{\tau}_c$ are the modified torques, taking $\hat{\tau}_l = \tau_l - \tau_{c0}$ and $\hat{\tau}_c = \tau_c - \tau_{c0}$ for the equilibrium τ_{c0}. The compressor torque τ_c can be formulated as:

$$\tau_c = \frac{D_2^2\sigma}{2D_1}\text{sgn}(m)mU_1 \tag{3.8}$$

To ensure continuity, a scaled hyperbolic tangent function will be used:

$$\tau_c = \frac{D_2^2\sigma}{2D_1}\tanh\left(\frac{m}{\varsigma}\right)mU_1 \tag{3.9}$$

where $\varsigma > 0$ is a sufficiently large constant. τ_c can now be formulated as:

$$\begin{aligned}\tau_c &= \frac{D_2^2\sigma}{2D_1}\tanh\left(\frac{m}{\varsigma}\right)(\hat{m} + m_0)(\hat{U} - U_d)\\ &= \underbrace{\frac{D_2^2\sigma}{2D_1}\tanh\left(\frac{m}{\varsigma}\right)(\hat{m} + m_0)(\hat{m}\hat{U} + \hat{m}U - d + m_0\hat{U})}_{\hat{\tau}_c}\\ &\quad + \underbrace{\frac{D_2^2\sigma}{2D_1}\tanh\left(\frac{m}{\varsigma}\right)m_0U_d}_{\tau_{c0}}\end{aligned} \tag{3.10}$$

Now the control theorem can be formulated according to (Gravdahl and Egeland, 1999):

Theorem 3.1. *The surge control law*

$$\Psi_v = k_v \hat{m} \tag{3.11}$$

and speed control law

$$\begin{aligned} \hat{\tau}_l &= -k_p \hat{U} - k_i \hat{I} \\ \dot{\hat{I}} &= \hat{U} \end{aligned} \tag{3.12}$$

with

$$k_p > 0, k_i > 0 \text{ and } k_v > \sup_{\hat{U},\hat{m}} \left\{ \frac{\delta \hat{\Psi}_c(\hat{m}, \hat{U})}{\delta \hat{m}} \right\} + \delta_1 \tag{3.13}$$

and $\delta_1 > 0$ make the origin of Equation 3.7 semi-global exponentially stable. The desired speed $\hat{U}_d$ is therefore reached for the equilibrium to the left or to the right of the original surge line. The integral term in Equation 3.12 is added to robustify the controller with respect to un-modeled disturbance torques.

Proof:

The proof from (Gravdahl and Egeland, 1999) is modified here to fit the exact model used in this thesis. Define

$$n \triangleq \begin{pmatrix} \hat{U} \\ \hat{I} \end{pmatrix} \text{ and } \mathbf{P} \triangleq \begin{pmatrix} \frac{2I}{D_1} & \lambda \\ \lambda & k_i \end{pmatrix} \tag{3.14}$$

where $\lambda > 0$ and $k_i > 0$ are design parameters. Consider then the following Lyapunov function candidate:

$$V(\hat{p}, \hat{m}, \hat{U}, \hat{I}) = \frac{1}{2}(V_p + V_m + V_{spool}) \tag{3.15}$$

where

$$\begin{aligned} V_p &= \frac{V_p}{a_{01}^2 \rho_{01}} \hat{P}^2 \\ V_m &= \frac{L}{A_1 \rho_{01}} \hat{m}^2 \\ V_{spool} &= n^T \mathbf{P} n \end{aligned} \tag{3.16}$$

Since all of the coefficients in Equation 3.15 are constant, V will be positive definite and radially unbounded if λ is chosen such that $P > 0$, meaning:

$$\lambda < \sqrt{\frac{2Ik_i}{D_1}} \tag{3.17}$$

The time derivative of Equation 3.15 along the solutions of Equation 3.7 gives:

$$\begin{aligned}\dot{V} &= \hat{m}\left(\hat{\Psi}_c(\hat{m},\hat{U}) - \hat{\Psi}_v(\hat{m})\right)\frac{p_{01}}{\rho_{01}} - \frac{1}{\rho_{01}}\hat{p}\hat{m}_{out}(\hat{p}) - k_p\hat{U}^2 \\ &+\lambda\hat{U}^2 - \tfrac{\lambda k_i D_1}{2I}\hat{U}\hat{I} - \hat{U}\hat{\tau}_c - \tfrac{\lambda D_1}{2I}\hat{I}\hat{\tau}_c\end{aligned} \tag{3.18}$$

An upper bound for the last term in Equation 3.18 is:

$$\begin{aligned}-\frac{\lambda D_1}{2I}\hat{I}\hat{\tau}_c &= -\frac{\lambda D_2^2\sigma}{4I}\left(\tanh\left(\frac{m}{\varsigma}\right)\hat{m}U + m_0\hat{U}\right)\hat{I} \\ &\leq \frac{\lambda D_2^2\sigma}{4I}\left(\frac{U_m}{2}\left(\frac{\hat{m}^2}{\eta_1} + \eta_1\hat{I}^2\right) + m_0\hat{U}\hat{I}\right)\end{aligned} \tag{3.19}$$

using Young's inequality. The parameter $\eta_1 > 0$ can be chosen freely. An upper bound for the term $\hat{U}\hat{\tau}_c$ is then:

$$\begin{aligned}-\hat{U}\hat{\tau}_c &= -\frac{D_2^2\sigma}{2D_1}\tanh\left(\frac{m}{\varsigma}\right)\left((\hat{m}+m_0)\hat{U} + \hat{m}U_d\right)\hat{U} \\ &\leq -\frac{D_2^2\sigma}{2D_1}\tanh\left(\frac{m}{\varsigma}\right)m\hat{U}^2 + \frac{D_2^2\sigma}{4D_1}\left(\frac{\hat{m}^2}{\eta_2} + \eta_2(U_d\hat{U})^2\right)\end{aligned} \tag{3.20}$$

Based on Equation 3.19 and Equation 3.20 an upper bound for Equation 3.18 can be found as:

$$\begin{aligned}\dot{V} \leq\ & \hat{m}\left(\hat{\Psi}_c(\hat{m},\hat{U}) - \hat{\Psi}_v(\hat{m})\right)\frac{p_{01}}{\rho_{01}} - \frac{D_2^2\sigma}{2D_1}\tanh\left(\frac{m}{\varsigma}\right)m\hat{U}^2 \\ &+\left(\frac{\sigma\lambda D_2^2 U_m}{8I\eta_1} + \frac{D_2^2\sigma}{4D_1\eta_2}\right)\hat{m}^2 - \frac{1}{\rho_{01}}\hat{p}\hat{m}_{out}(\hat{p}) - n^T\mathbf{Q}n\end{aligned} \tag{3.21}$$

where

$$\mathbf{Q} = \begin{bmatrix} k_p - \lambda - \frac{D_2^2\sigma U_d^2\eta_2}{4D-1} & \frac{\lambda}{4I}\left(D_1k_p - \frac{\sigma D_2^2 m_0}{2}\right) \\ \frac{\lambda}{4I}\left(D_1k_p - \frac{\sigma D_2^2 m_0}{2}\right) & \frac{\lambda}{2I}\left(k_iD_1 - \frac{\sigma D_2^2 U_m\eta_1}{4}\right)\end{bmatrix} \tag{3.22}$$

For $\mathbf{Q} > 0$, k_p, η_1 and λ must be chosen as:

$$k_p > \frac{D_2^2\sigma U_d^2\eta_2}{4D_1} \tag{3.23}$$

$$\eta_1 < \frac{4k_iD_1}{\sigma D_2 U_m} \tag{3.24}$$

and

$$\lambda < \min\{\lambda_1, \lambda_2\} \tag{3.25}$$

with

$$\lambda_1 = k_p - \frac{D_2^2 \sigma U_d^2 \eta_2}{4 D_1} \tag{3.26}$$

and

$$\lambda_2 = \frac{\left(k_p - \frac{D_2^2 \sigma U_d^2 \eta_2}{4 D_1}\right)\left(k_i D_1 - \frac{\sigma D_2 U_m \eta_1}{4}\right)}{k_i D_1 - \frac{\sigma D_2 U_m \eta_1}{4} + \frac{1}{8I}\left(D_1 k_p - \frac{\sigma D_2 m_0}{2}\right)^2} \tag{3.27}$$

where m_{out} is assumed to satisfy the sector condition:

$$\hat{p}\hat{m}_{out}(\hat{p}) > \delta_2 \hat{p}^2 \tag{3.28}$$

meaning that the throttle valve is assumed passive. Because $\hat{p}\hat{m}_{out}(\hat{p})$ is of the order $\frac{3}{2}$, Equation 3.28 will not hold globally. This can be handled by introducing a given $\hat{p}_{max}$, leading to:

$$|\hat{p}(t)| \leq \hat{p}_{max} \forall t > 0 \tag{3.29}$$

It will then always be possible to choose δ_2 small enough for Equation 3.28 to hold for $|\hat{p}(t)| \leq \hat{p}_{max}$. The pressure drop $\hat{\Psi}_v(\hat{m})$ over the CCV must be chosen such that the first term in Equation 3.21:

$$-\hat{m}\left(\hat{\Psi}_c(\hat{m}, \hat{U}) - \hat{\Psi}_v(\hat{m})\right)\frac{p_{01}}{\rho_{01}} > 0 \forall \hat{U}, \tag{3.30}$$

is satisfied. Sufficient conditions for Equation 3.30 to hold, since $\frac{p_{01}}{\rho_1} > 0$, are:

$$-\left(\hat{\Psi}_c(\hat{m}, \hat{U}) - \hat{\Psi}_v(\hat{m})\right)\Big|_{\hat{m}=0} = 0 \tag{3.31}$$

and

$$\frac{\partial}{\partial \hat{m}}\left(\hat{\Psi}_c(\hat{m}, \hat{U}) + \hat{\Psi}_v(\hat{m})\right) > 0. \tag{3.32}$$

With

$$\hat{\Psi}_c(0, \hat{U}) = \hat{\Psi}_c(m_0, U_d) - \hat{\Psi}_c(m_0, U_d) = 0 \tag{3.33}$$

$$\hat{\Psi}_v(\hat{m}) = k_v \hat{m} \Rightarrow \hat{\Psi}_v(0) = 0, \tag{3.34}$$

Equation 3.31 will then be satisfied. Moreover, Equation 3.32 yields:

$$-\frac{\partial}{\partial \hat{m}}\hat{\Psi}_c(\hat{m}, \hat{U}) + k_v > 0 \tag{3.35}$$

If k_v is chosen according to:

$$k_v > \sup_{\hat{U},\hat{m}} \left\{ \frac{\partial \hat{\Psi}_c(\hat{m},\hat{U})}{\partial \hat{m}} \right\} \tag{3.36}$$

Equation 3.32 will be satisfied, thereby ensuring that Equation 3.30 is satisfied. Choosing k_v as:

$$k_v > \sup_{\hat{U},\hat{m}} \left\{ \frac{\partial \hat{\Psi}_c(\hat{m},\hat{U})}{\partial \hat{m}} \right\} + \delta_1 \tag{3.37}$$

where $\delta_1 > 0$, means that $\hat{m}\Psi_v(\hat{m}) > \delta_1 \hat{m}^2$ holds. Equation 3.30 can be rearranged to:

$$-\hat{m}\left(\hat{\Psi}_c(\hat{m}),\hat{U}) - \hat{\Psi}_v(\hat{m})\right)\frac{p_{01}}{\rho_{01}} > \frac{p_{01}}{\rho_{01}}\delta_1 \hat{m}^2 \forall \hat{U} \tag{3.38}$$

The upper bound for $\dot{V}$ can now be formulated as:

$$\dot{V} \leq \left(\frac{p_{01}}{\rho_{01}}\delta_1 - \frac{\sigma\lambda D_2^2 U_m}{8I\eta_1} - \frac{D_2^2\sigma}{4D_1\eta_2}\right)\hat{m}^2 - \delta_2\hat{p}^2 - \frac{1}{2}n^T\mathbf{Q}n \;\forall \hat{m},\hat{p},n \tag{3.39}$$

An upper bound for the cross terms of $\hat{U}$ and $\hat{I}$ can be found using Young's inequality:

$$\lambda\hat{U}\hat{I} \leq \frac{\lambda}{2}\left(\frac{\hat{U}^2}{\eta_3} + \eta_3\hat{I}^2\right) \tag{3.40}$$

$$-\frac{\lambda(4D_1k_p - \sigma D_2^2 m_0)}{2I}\hat{U}\hat{I} \leq \frac{\lambda(4D_1k_p - \sigma D_2^2 m_0)}{4I}\left(\frac{\hat{U}^2}{\eta_4 + \eta_4\hat{I}^2}\right) \tag{3.41}$$

where $\eta_3 > 0$ and $\eta_4 > 0$ are freely chosen constants. Comparing the coefficients in Equation 3.40 and Equation 3.15 using Equation 3.40 and Equation 3.41 leads to the following expressions, provided that the inequalities hold:

$$\begin{aligned}
\delta_1 - \frac{\sigma\lambda D_2^2 U_m \rho_{01}}{8I\eta_1 p_{01}} - \frac{D_2^2\sigma\rho_{01}}{4D_1\eta_2 p_{01}} &> \varpi\frac{L}{A\rho_{01}} \\
\delta_2 &> \varpi\frac{V_p}{a_{01}^2\rho_{01}} \\
k_p - \lambda - \frac{\lambda(4D_1k_p - \sigma D_2^2 m_0)}{4I\eta_4} &> \varpi\left(\frac{I}{D_1} + \frac{\lambda}{2\eta_3}\right) \\
\lambda k_i - \frac{\lambda(4D_1k_p - \sigma D_2^2 m_0}{4I}\eta_4 &> \varpi\left(\frac{k_i}{D_1} + \frac{\varpi\eta_3}{2}\right)
\end{aligned} \tag{3.42}$$

For a constant $\varpi > 0$, the following holds:

$$\dot{V} \leq -\varpi V \Rightarrow V(t) \leq V(0)e^{-\varpi t} \tag{3.43}$$

If η_1 is chosen according to Equation 3.24, δ_1 chosen as:

$$\delta_1 > \frac{\sigma \lambda D_2^2 U_m \rho_{01}}{8I\eta_1 p_{01}} + \frac{D_2^2 \sigma \rho_{01}}{4D_1 \eta_2 p_{01}} \tag{3.44}$$

,k_v is chosen according to Equation 3.37 and λ is chosen according to Equation 3.17, Equation 3.25 will ensure that Equation 3.42 is satisfied for some $\varpi > 0$. It then follows from Equation 3.43 the origin of Equation 3.7 is exponentially stable. Based on the assumption embedded in Equation 3.29, this result holds when $|\hat{p}(0)| \leq \hat{p}_{max}$, thereby making the origin semi globally exponentially stable. □

3.2 Simulation results for CCV

The dynamic equations given by Equation 3.7 are implemented in SIMULINK, according to the scheme outlined in Figure 3.2.

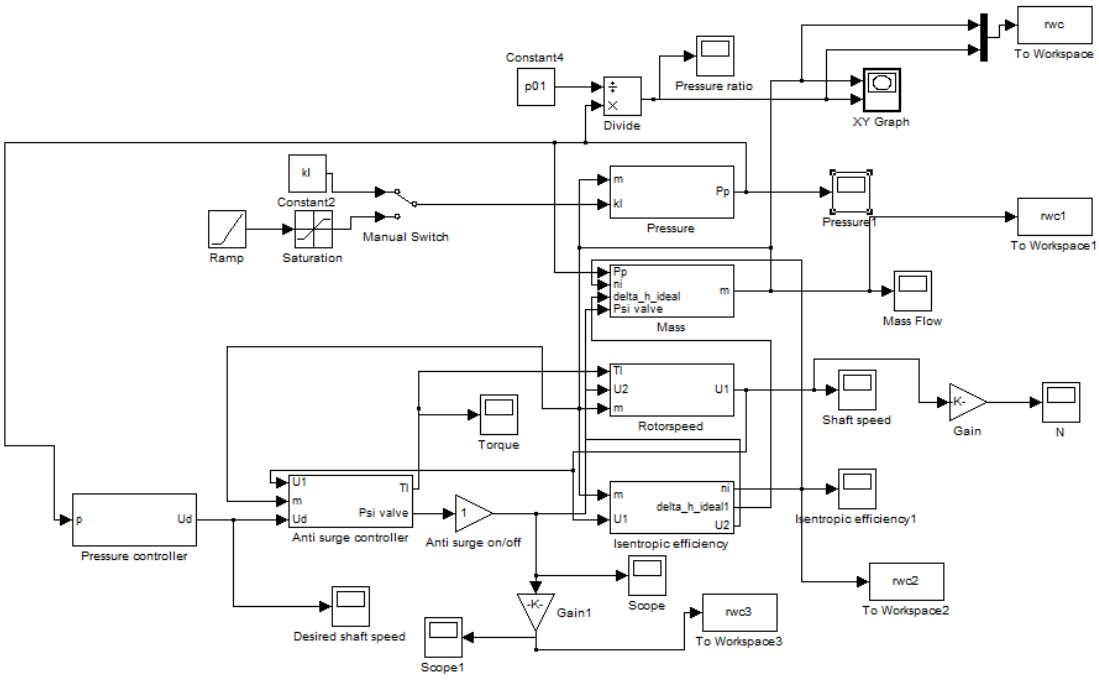

Figure 3.2: Dynamic equations of compressor fitted with CCV and implemented in SIMULINK.

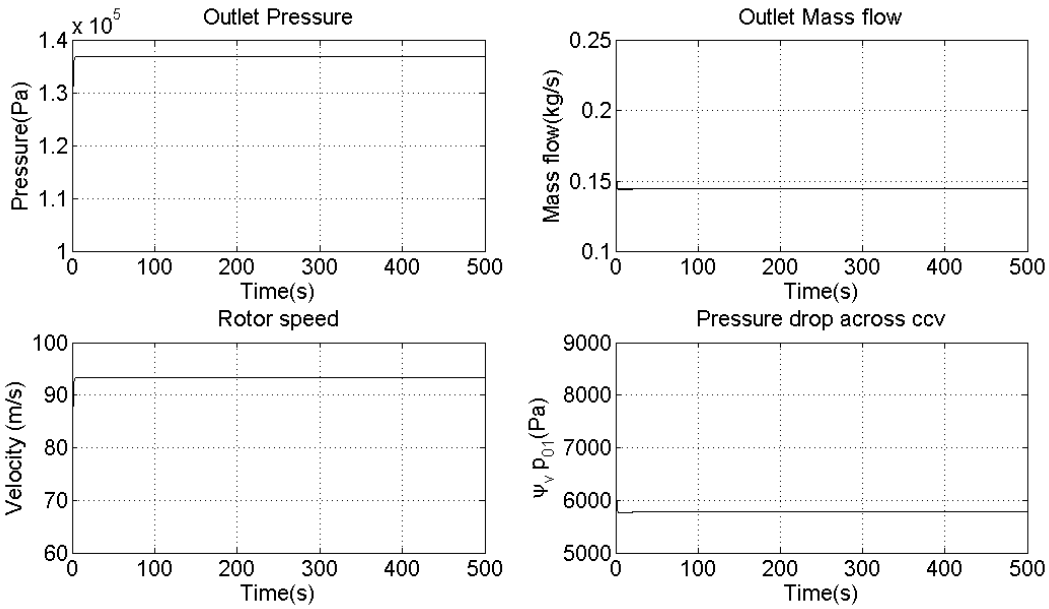

Figure 3.3: Outlet pressure, mass flow, rotor speed and pressure drop across CCV with surge controller enabled.

It can be seen from Figure 3.2 that the controllers work in a cascade form. This means that the desired setpoint for the rotor speed, $\hat{U}_d$ is calculated based on a desired setpoint for outlet pressure, denoted p_0. This value is set to $137 \cdot 10^5 Pa$. The anti-surge controller block contains both the CCV-controller from Equation 3.11 and the torque controller based on a PID-controller. All of the variables used in the simulation of this model can be found in Appendix D. The simulation is carried out for 500 seconds. This is to ensure that a possible surge cycle will have enough time to develop if the active surge-controller fails to stabilize the compressor. Three different simulations have been carried out. The first demonstrates the CCV-controller for avoiding surge, the second is the same test, but without the CCV-controller. In the third test, a delay in the mass flow measurement fed to the surge controller is added to the system. These tests will make it possible to evaluate the active surge control scheme. All simulations are run with a fixed throttle gain, $k_l = 0.0007$.

Figure 3.3 shows the result of the simulation run with the surge controller switched on. The outlet pressure is $137 \cdot 10^5 Pa$, which is the same as the reference value. The spikes observed in the beginning of the simulations are a result of that the system is instantaneously switched on. Normally, a start-up sequence would be performed

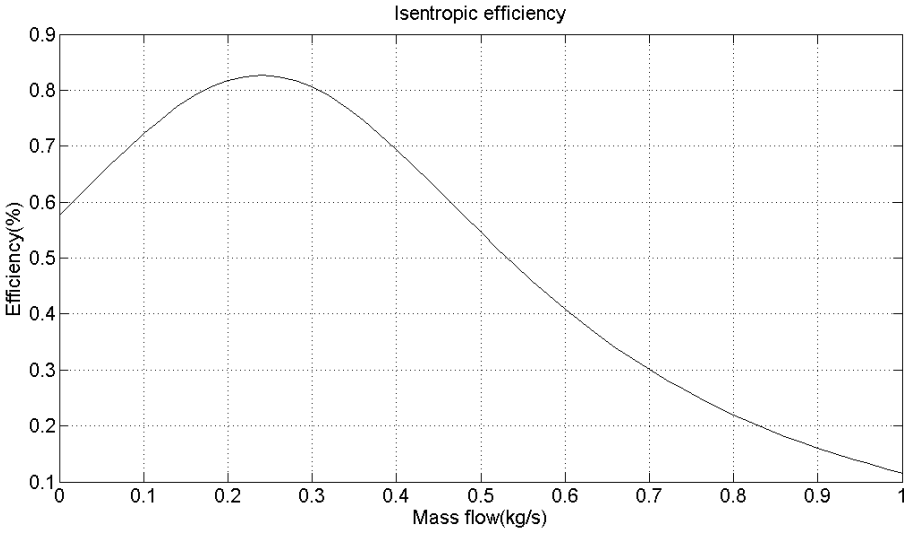

Figure 3.4: Variation in isentropic efficiency with mass flow.

on the compressor to avoid damage. The pressure drop across the CCV is about $5700Pa$, corresponding to about 0.04% of the outlet pressure. This means that very little energy is required to compensate this loss.

The isentropic efficiency of the compressor is a measure of how much of the energy consumption of the compressor that actually is used to increase the pressure of the fluid, and how much is lost due to friction and heat. The peak of the isentropic efficiency coincides with the point of surge, meaning that at the point of surge, this compressor operates at its maximum efficiency. Figure 3.4 shows that the peak of the efficiency occurs at a mass flow rate of approximately $0.24\frac{kg}{s}$. This is the same mass flow being observed at the peak of the 50000 rpm line in Figure 2.1. It should be noted that the peak of efficiency and point of surge do not necessarily coincide. In the work of (Grong and Kylling, 2008), the peak efficiency of the compressor on the Snorre A platform was designed to be far away from the point of surge. The impact of this designed move is not known. This matter has been discussed with Professor Gravdahl. But for the compressor studied in this thesis, the argument of operating the compressor at the point of surge for maximum isentropic efficiency is valid.

In Figure 3.5 the effect of a surge is simulated. Both the pressure and mass flow oscillate, and flow reversal occurs in the compressor. This is what all surge controllers seek to avoid, since it is clear that a fluid flowing in such a manner will damage both

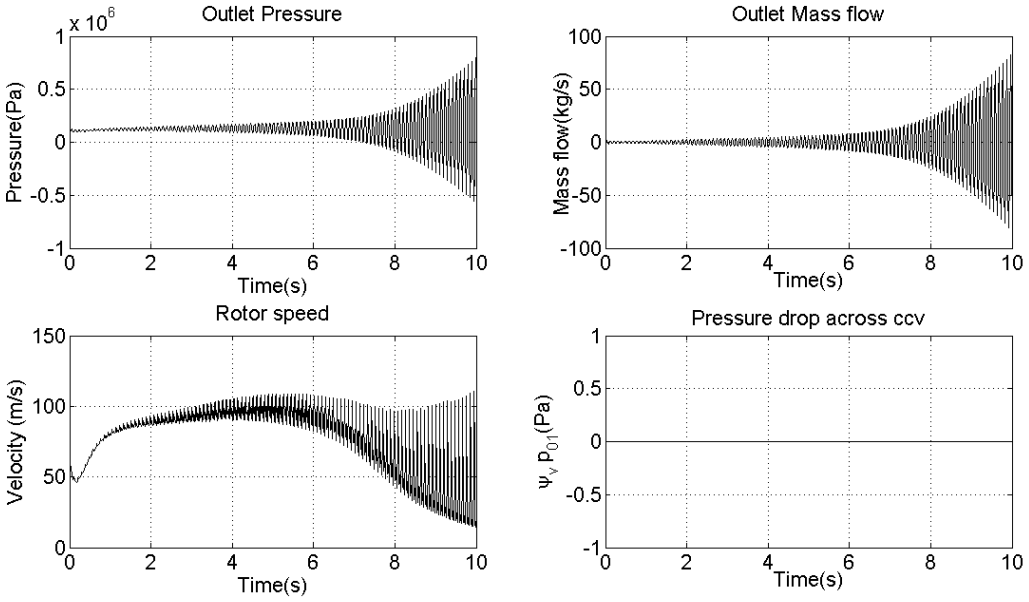

Figure 3.5: Outlet pressure, mass flow, rotor speed and pressure drop across CCV with surge controller disabled.

the compressor and equipment upstream and downstream. The disabling of the CCV-controller is what triggers the surge. With the exception of the CCV-controller, all settings and variables are the same as those used in the simulation shown previously in Figure 3.3.

Figure 3.6 shows the result of introducing a transport delay of $50ms$ on the mass flow measurement to the CCV-controller. All settings and variables are the same as those used in the simulation shown previously in Figure 3.3. The small delay makes the controller unable to react fast enough to keep the compressor out of surge. The pressure drop over the CCV is not changed fast enough to stabilize the compressor characteristic, and surge is thus induced in the compressor. The effect of a simple measurement delay illustrates one of the current, major problems with this active surge controller. This is confirmed by (van Helvoirt, 2007) and (Grong and Kylling, 2008). Since all measurement equipment has a certain delay (e.g. the mass flow meter used by (van Helvoirt, 2007) had a 2 second measurement delay), the inability to deal with this delay must be addressed before the CCV can be used in an industrial compressor system. The CCV solution will be further evaluated and discussed later.

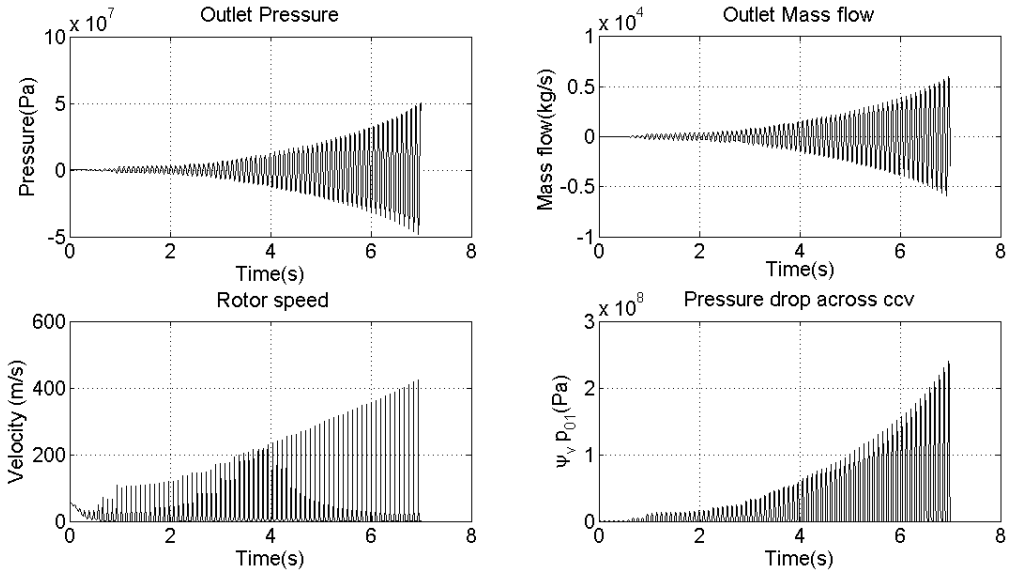

Figure 3.6: Outlet pressure, mass flow, rotor speed and pressure drop across CCV with surge control enabled and a delay in the mass flow measurement to the controller.

Chapter 4

Drive torque actuation

Another promising way of achieving active surge control is to use the drive torque from the engine running the rotor of the compressor to compensate the mass flow fluctuations which otherwise would lead to surge. This design is presented in (Gravdahl et al., 2002) and (Bøhagen, 2007). Control laws for using either the impeller speed or the torque as control input are presented below.

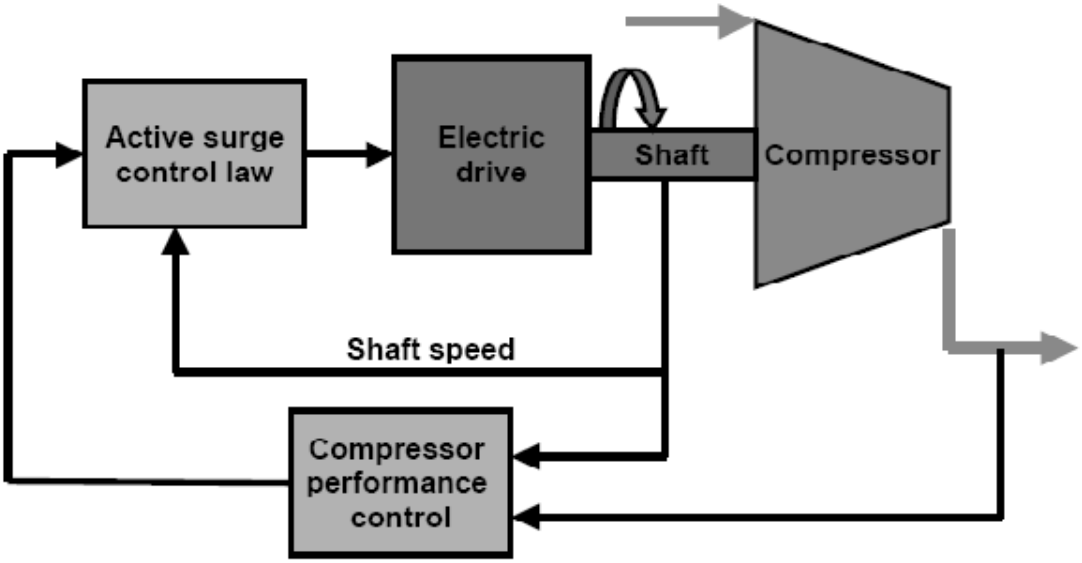

Figure 4.1: Compressor system with electrical drive. From (Gravdahl et al., 2002).

Figure 4.1 shows a compressor system fitted with an electrical motor as a drive unit. This is opposed to gas turbine driven compressors, which are more commonly

used in offshore processing systems.

4.1 Drive torque control law

The first theorem presents a control law for the impeller speed. The compressor model used in these calculations is the one from Equation 3.7. The theorem and proof are from (Gravdahl et al., 2002), modified here to comply with the current model.

Theorem 4.1. *The control law:*

$$\hat{U} = -c\hat{m} \tag{4.1}$$

where the gain c is chosen according to:

$$c > \frac{\delta\psi_c/\delta m}{\delta\psi_c/\delta U} \tag{4.2}$$

makes the origin of Equation 3.7 globally exponentially stable.

Proof.

Consider the Lyapunov function candidate:

$$V = \frac{V_p}{2a_{01}^2}\hat{p}^2 + \frac{L}{2A}\hat{m}^2 > 0, \forall(\hat{m},\hat{p}) \neq (0,0) \tag{4.3}$$

Derivation of Equation 4.3 with respect to time along the solution of Equation 3.7 gives:

$$\dot{V} = \frac{a_{01}^2}{V_p}\hat{p}\dot{\hat{p}} + \frac{L}{A}\hat{m}\dot{\hat{m}} = \hat{p}(\hat{m} - \hat{m}_t) + \hat{m}(\hat{\psi}_c p_{01} - \hat{p}) \tag{4.4}$$

The time derivative can then be formulated as:

$$\dot{V} = \dot{V}_1 + \dot{V}_2 = -\hat{p}\hat{m_{out}}(\hat{p}) + \hat{m}\hat{\Psi}_c(\hat{m},\hat{U})p_{01} \tag{4.5}$$

The throttle valve is assumed to be passive, i.e. it consumes energy from the compressor. This leads to:

$$\dot{\hat{V}_1} = -\hat{p}\hat{m_{out}}(\hat{p}) < -k_p\hat{p}^2 < 0, \forall\hat{p} \neq 0 \tag{4.6}$$

where $k_p > 0$ depends on the slope of the compressor characteristic. In order to prove stability, $\hat{V_2} = \hat{m}\hat{\Psi}_c(\hat{m}, \hat{U})p_{01} < 0$ when $\hat{U}$ is chosen as in Equation 4.1. Since $\hat{\Psi}_c(\hat{m}, -c\hat{m})|_{\hat{m}=0} = 0$, a sufficient condition for $\hat{\Psi}_c(\hat{m}, \hat{U})$ to be located within the 2^{nd} and 4^{th} quadrant in the $(\hat{m}, \hat{\Psi}_c)$ coordinate system is that $\hat{\Psi}_c(\hat{m}, \hat{U})|_{\hat{U}=-c\hat{m}}$ is monotonically *decreasing*. This means:

$$\frac{d\hat{\Psi}_c(\hat{m}, \hat{U})}{d\hat{m}} = \frac{\partial\hat{\Psi}_c}{\partial\hat{m}} + \frac{\partial\hat{\Psi}_c}{\partial\hat{U}}\frac{\partial\hat{U}}{\partial\hat{m}} = \frac{\partial\hat{\Psi}_c}{\partial\hat{m}} - c\frac{\partial\hat{\Psi}_c}{\partial\hat{U}} < 0 \tag{4.7}$$

Then, based on Equation 4.1 it follows that:

$$c > \frac{\partial\hat{\Psi}_c/\partial\hat{m}}{\partial\hat{\Psi}_c/\partial\hat{U}} = \frac{\partial\hat{\Psi}_c/\partial\hat{m}}{\partial\hat{\Psi}_c/\partial\hat{U}} \tag{4.8}$$

where the first equality comes from the coordinate shifts in Equation 3.6. The choice of c according to Equation 4.8 satisfies the condition from Equation 4.7. This makes $\hat{\Psi}_c(\hat{m}, \hat{U})\big|_{\hat{U}=-c\hat{m}}$ monotonically decreasing and passing through the origin, located in the 2^{nd} and 4^{th} quadrant. Multiplying $\hat{\Psi}_c(\hat{m}, \hat{U})|_{\hat{U}=-c\hat{m}}$ with $\hat{m}$, where $\hat{m}$ belongs to the 1^{st} and 3^{rd} quadrant, gives:

$$\dot{V_2} = \hat{m}\hat{\Psi}_c(\hat{m}, -c\hat{m})p_{01} < 0, \forall\hat{m} \neq 0 \tag{4.9}$$

V_2 can be bound from above with:

$$\dot{V_2} = \hat{m}\hat{\Psi}_c(\hat{m}, -c\hat{m})p_{01} < -k_m\hat{m}^2, \forall\hat{m} \neq 0 \tag{4.10}$$

where $k_m > 0$. From Equation 4.10 it follows that:

$$\hat{\Psi}_c(\hat{m}, -c\hat{m})p_{01} < -k_m\hat{m}, \hat{m} > 0 \tag{4.11}$$

Because $\hat{\Psi}_c(\hat{m}, -c\hat{m})p_{01}$ is monotonically decreasing and passing through the origin, it is also bound by the tangent passing through the origin:

$$\hat{\Psi}_c(\hat{m}, -c\hat{m})p_{01} < p_{01}\frac{d\hat{\Psi}_c(\hat{m}, -c\hat{m})}{d\hat{m}}\hat{m} \tag{4.12}$$

If k_m is chosen as:

$$k_m = -p_{01}\frac{d\hat{\Psi}_c(\hat{m}, -c\hat{m})}{d\hat{m}}\bigg|_{\hat{m}=0} \tag{4.13}$$

From this Equation 4.10 and Equation 4.11 are satisfied. Similar calculations can also be done for the case of $\hat{m} < 0$. Equation 4.3, Equation 4.6 and Equation 4.10 then give:

$$\dot{V} = \dot{V_1} + \dot{V_2} < -k_p\hat{p}^2 - k_m\hat{m}^2 < -kV, \forall(\hat{m}, \hat{p}) \neq (0, 0) \tag{4.14}$$

where

$$k < min\left\{\frac{k_p}{\frac{V_p}{2a_{01}^2}}, \frac{k_m}{\frac{L}{2A}}\right\} \tag{4.15}$$

and the result follows. □

The control law in Equation 4.1 ensures that the compressor characteristics have a negative slope at equilibrium. In practice, this will have the same effect as the one achieved by using the CCV approach, but without a pressure drop over the CCV.

The stability of the system will be presented by introducing shaft dynamics. Derivation of the Lyapunov function candidate in Equation 4.3 with respect to time along the trajectories of Equation 3.7 yields:

$$\dot{V} < -k_m\hat{p}^2 - k_m\hat{m}^2 + \hat{m}\delta(t) \tag{4.16}$$

where $\delta(t) = \frac{A}{L}\tilde{\Psi}_c(t)$ and $\tilde{\Psi}_c := \Psi_c(m, U) - \Psi_c(m, U - d)$ are the total error in the pressure rise in Ψ_c because of the shaft dynamics when the speed U converges to its desired value $U_d = U_0 - c\hat{m}$. It can be seen from Equation 4.16 that the system converges towards a set $\mathcal{A}_1$ when

$$k_m|\hat{m}| > |\delta(t)| \tag{4.17}$$

Using Young's inequality on the last term in Equation 4.16 yields:

$$\hat{m}\delta(t) < \nu_1\hat{m}^2 + \frac{\delta^2(t)}{4\nu_1} < \nu_1\hat{m}^2 + \frac{\|\delta\|_\infty^2}{4\nu_1}, \forall\nu_1 > 0 \tag{4.18}$$

where ν_1 is a constant. Equation 4.16 can the be rewritten as:

$$\dot{V} < -k_p\hat{p}^2 - (k_m - \nu_1)\hat{m}^2 + \frac{\|\delta\|_\infty^2}{4\nu_1} = -W(\hat{x}) + \frac{\|\delta\|_\infty^2}{4\nu_1} \tag{4.19}$$

where $\hat{x} = \binom{\hat{p}}{\hat{m}}$ and $W(\hat{x})$ are positive definite and radially unbounded if ν_1 is chosen such that $\nu_1 < k_m$.

$V(\hat{x})$ as given by Equation 4.3 and $W(\hat{x})$ as given by Equation 4.19 are quadratic, positive definite, radially unbounded and smooth. Because of this there exists a quadratic bound such that:

$$\begin{aligned} \beta_1||\hat{x}||^2 \leq V(\hat{x}) \leq \beta_1||\hat{x}||^2 \\ \beta_3||\hat{x}||^2 \leq W(\hat{x}) \end{aligned} \tag{4.20}$$

where β_1, β_2 and β_3 are positive constants. From Equation 4.3 it is seen that $V = \hat{x}^T\mathbf{R}\hat{x}$, with $\mathbf{R}$ as the positive definite matrix:

$$\mathbf{R} = \begin{bmatrix} \frac{V_p}{2a_{01}^2} & 0 \\ 0 & \frac{L}{2A} \end{bmatrix} \tag{4.21}$$

Then β_1 and β_2 can be written $\beta_1 = \underline{\lambda}_R$ and $\beta_2 = \overline{\lambda}_R$, where $\underline{\lambda}_R = \min\left\{\frac{V_p}{2a_{01}^2}, \frac{L}{2A}\right\}$ and $\overline{\lambda}_R = \max\left\{\frac{V_p}{2a_{01}^2}, \frac{L}{2A}\right\}$ are the lower and upper eigenvalues of $\mathbf{R}$. $\beta_3 = \underline{\lambda}_Q$, where $\underline{\lambda}_Q = \min\{k_p, (k_m - \nu_1)\}$ can be found in a similar way. Then it follows from Equation 4.3, Equation 4.19 and Equation 4.20 that $\hat{x}(t)$ is globally uniformly bounded and converges to the compact set:

$$\mathcal{A}_1 = \left\{ \hat{x} : ||\hat{x}|| < \sqrt{\frac{\frac{\beta_2}{\beta_3}\frac{||\delta||_\infty^2}{4\nu_1}}{\beta_1}} \right\} = \left\{ \hat{x} : ||\hat{x}|| < \frac{1}{2}\sqrt{\frac{\beta 2}{\beta_1\beta_2\nu_1}}||\delta||_\infty \right\} \tag{4.22}$$

The compactness of $\mathcal{A}_1$ follows from the fact of the quadratic bounds in Equation 4.20. This is discussed in (Khalil, 2002). To determine the rate of convergence consider the signal:

$$s \triangleq V(\hat{x}e^{\gamma t}) \tag{4.23}$$

where γ is a constant. The time derivative of s can be upper bounded using Equation 4.19 and Equation 4.20 such that:

$$\begin{aligned} \frac{ds}{dt} &= \left(\dot{V} + \alpha V\right) e^{\gamma t} \\ &\leq \left(-W(\hat{x}) + \frac{\|\delta\|_\infty^2}{4\nu_1} + \alpha V\right) e^{\gamma t} \\ &\leq \left(-\beta_3||\hat{x}||^2 + \gamma\beta_2||\hat{x}||^2\right) e^{\gamma t} + \frac{\|\delta\|_\infty^2}{4\nu_1} e^{\gamma t} \end{aligned} \tag{4.24}$$

The choice of $\gamma \leq \frac{\beta_3}{\beta_2}$ makes:

$$\frac{ds}{dt} \leq \frac{\|\delta\|_\infty^2}{4\nu_1} e^{\gamma t} \tag{4.25}$$

By integrating Equation 4.25 an upper bound for $\hat{x}$ can be found:

$$\int_0^t \frac{ds}{dt}dt' \leq \int_0^t \frac{\|\delta\|_\infty^2}{4\nu_1}e^{\gamma t}dt'$$

$$\Downarrow$$

$$V(\hat{x}(t))e^{\gamma t} - V(\hat{x}(0)) \leq \frac{\|\delta\|_\infty^2}{4\nu_1}(e^{\gamma t} - 1) \tag{4.26}$$

$$V(\hat{x}(t)) \leq V(\hat{x}(0))e^{-\gamma t} + \frac{\|\delta\|_\infty^2}{4\nu_1}$$

Using Equation 4.20 and Equation 4.26 it then follows that:

$$\overline{\lambda}_R||\hat{x}(t)||^2 \leq \overline{\lambda}_R||\hat{x}(0)||^2e^{-\gamma t} + \frac{\|\delta\|_\infty^2}{4\nu_1}$$

$$||\hat{x}(t)|| \leq ||\hat{x}(0)||^2e^{-\frac{\gamma}{2}t} + \frac{\|\delta\|_\infty}{2\sqrt{\nu_1\overline{\lambda}_R}} \tag{4.27}$$

taking $\sqrt{a^2+b^2} \leq |a| + |b|$. From Equation 4.27 it follows that $\hat{x}(t)$ converges to the set $\mathcal{A}_1$ exponentially.

For velocity control, the engine torque can be generated by:

$$\tau_l = \hat{\tau} + \tau_0 \tag{4.28}$$

where $\tau_0 = \tau_{c0}$ is the torque required in the equilibrium point. The feedback control law is formulated as:

$$\hat{\tau} = K_1(U_d - U) \tag{4.29}$$

used to obtain the desired shaft speed:

$$U_d = U_0 - c\hat{m} \tag{4.30}$$

This gives the control law:

$$\tau_d = -K_1\hat{U} - K_2\hat{m} - K_1\int_0^t \hat{U}(t')dt' \tag{4.31}$$

where the feedback gain for the mass flow is given as:

$$K_2 = K_1c \tag{4.32}$$

The purpose of the integral term in Equation 4.31 is to generate the term τ_0. This will keep the compressor at the desired speed.

4.2 Simulation results for drive torque actuation

In this section the model as described by Equation 3.7 with the controller described by Equation 4.31 is implemented and tested in SIMULINK. The simulation is run for maximum 200 seconds in order to give a possible surge cycle enough time to develop. A saturation range of $0-3Nm$ and a rate limit of $\pm 5\frac{Nm}{s}$ is added to the output from the torque controller to simulate limitations for an electrical drive.

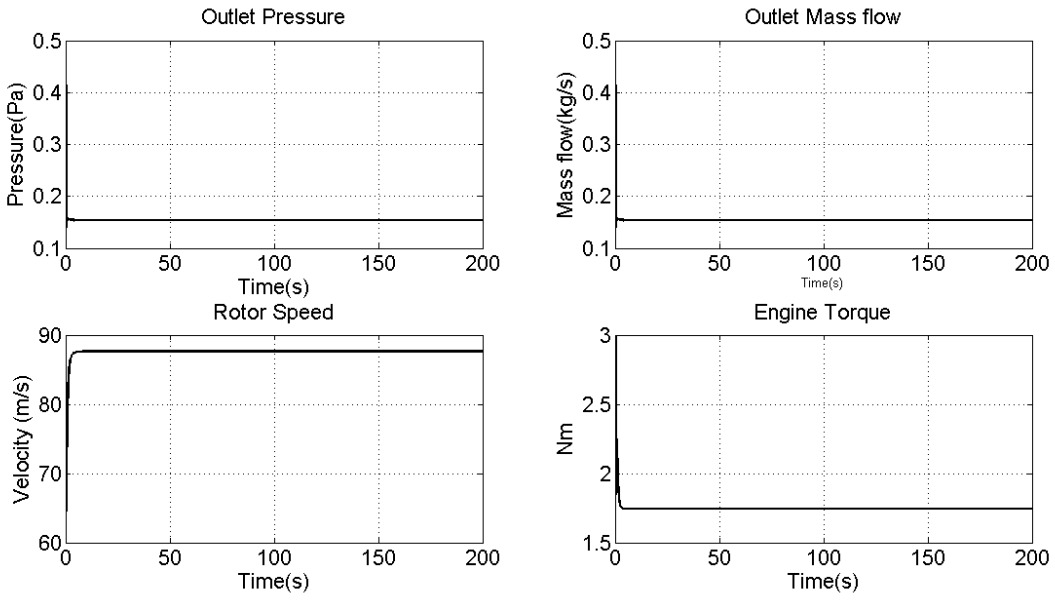

Figure 4.2: Outlet pressure, mass flow, rotor speed and torque as a function of time with correctly tuned torque controller.

Figure 4.2 shows the outlet pressure, mass flow, rotor speed and engine torque as a function of time with the torque controller tuned correctly according to Equation 4.15 and Equation 4.32. The controller gains K_1 and K_2 are set to 0.1 and 0.07, respectively. The pressure reaches the desired pressure of $137 \cdot 10^5 Pa$ almost immediately, and the system is stable, even if the mass flow is to the left of the surge line in the compressor characteristic in Figure 1.4. This means that the torque controller is able to keep the compressor out of surge.

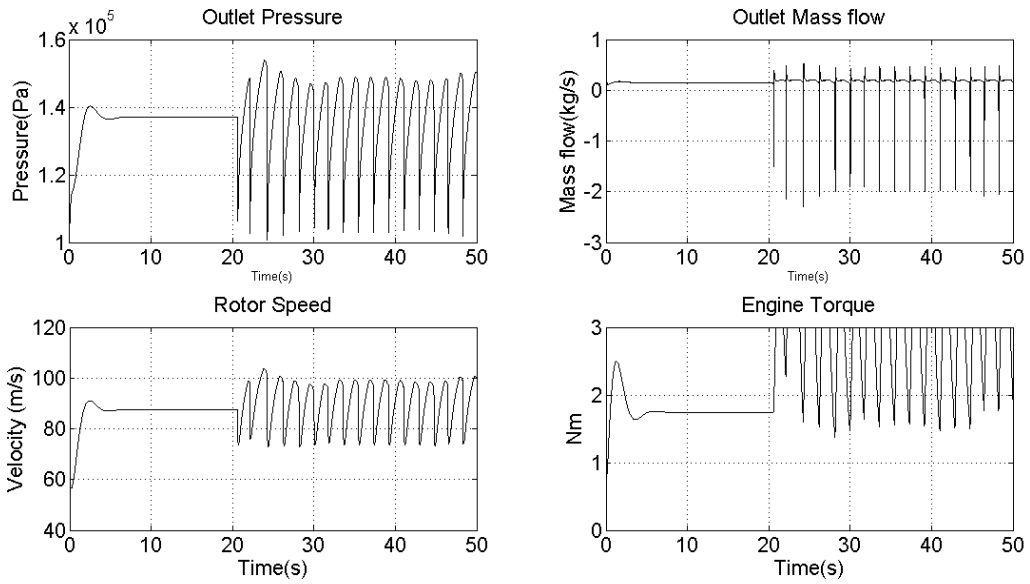

Figure 4.3: Outlet pressure, mass flow, rotor speed and torque as a function of time with badly tuned torque controller.

Figure 4.3 shows the outlet pressure, mass flow, rotor speed and engine torque as a function of time with the torque controller tuned badly, and not according to Equation 4.15 and Equation 4.32. The controller gain K_1 is set to 0.03, while K_2 is kept at 0.07. This makes the controller unable to keep the compressor out of surge. It starts out reasonably good, and reaches the desired pressure of $137 \cdot 10^5 Pa$ after about 7 seconds. But after about 20 seconds the controller reaches its limits and the surge cycle starts. This almost immediately results in flow reversal, as can be seen from the mass flow plot. This proves that the controller must be tuned correctly in order to keep the compressor out of surge, and insufficient and bad tuning can be disastrous. This also shows that surge is a time dependent problem and can develop after a certain period of time in a compressor system. Even after a successful startup sequence and a stable phase, the controller can reach its limit, thereby forcing the compressor to enter surge.

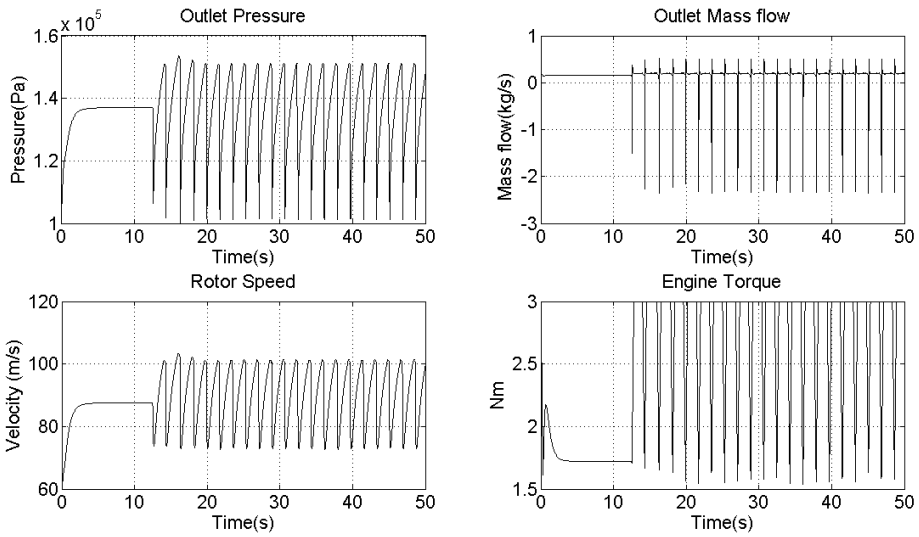

Figure 4.4: Outlet pressure, mass flow, rotor speed and torque as a function of time with a mass flow measurement delay implemented.

Figure 4.4 shows the outlet pressure, mass flow, rotor speed and engine torque as a function of time with the torque controller tuned correctly according to Equation 4.15 and Equation 4.32. The controller gains K_1 and K_2 are set to 0.1 and 0.07, respectively. The difference from the simulation in Figure 4.2 is that a measurement delay of $50ms$ is added to the mass flow measurement being fed to the torque controller. This makes the controller unable to keep the compressor out of surge, and the surge cycle begins after approximately 12 seconds. A measurement delay, always present in measurement equipment, will make the torque controller unable to react fast enough to changes in the operating conditions inside the compressor. This is the same type of problem that the CCV controller is facing. Active surge controllers rely on fast acting actuators and minimally delayed measurements.

Chapter 5

Comparison of active surge controllers and state observers

Based on the simulations and the requirements for the two solutions of an active surge controller, it is possible to give a recommendation on which of the two solutions that is the most promising one and should thus be the focus for further study. (van Helvoirt, 2007) and (Bøhagen, 2007) show that there is an ongoing work on both solutions. But they try to accomplish the same thing, and it would therefore be beneficial to eliminate one of the solutions, and focus all attention on the most promising one. This will ensure that the research effort is not wasted on investigating problems with one solution already being solved by others. Both solutions have industrial interest. (van Helvoirt, 2007) worked with Siemens in The Netherlands, (Bøhagen, 2007) with ABB in Norway, and (Grong and Kylling, 2008) with Siemens Technology and Innovation in Norway. The outlook of an improved and cost-saving surge controller makes it an interesting field of research for industrial companies. It is important to note that drive torque actuation is covered by the Norwegian patent held by Professor Gravdahl and ABB, see (ABB Research Ltd, 2000).

5.1 Solutions for active surge control

The simulations for the two solutions in the first case, with the controllers active and no measurement delays being implemented, prove that both controllers are able to stabilize the compressor systems within the unstable region of the compressor characteristic. This is not very surprising given that the control laws and the proofs hold. Both controllers behave adequately. But the CCV approach introduces a pressure

drop across the valve, which the engine must compensate in order to reach the desired outlet pressure. This means that the energy requirement for a compressor fitted with a CCV is larger than for a drive torque system. However, in this case, where the pressure drop across the valve is 0.04% of the outlet pressure, the increased energy consumption is negligible. In a larger compressor system, the pressure drop can be larger, and the increased energy consumption can have a stronger impact on the running costs of the compressor. This problem is avoided by the use of the drive torque solution. The second simulation carried out on the two solutions demonstrates what will happen if the controller is disabled.

The third simulation of both solutions shows that the addition of a measurement delay on the mass flow input to the controller has a dramatic impact on the performance of the systems. In both cases a transport delay of $50ms$ is added to the controller input. Figure 3.6 and Figure 4.4 show that the controllers are no longer able to stabilize the compressor systems. When operating within the unstable region of the compressor characteristic, the controller has very little tolerance for a delayed measurement. It is the delay itself that causes this. On the other hand, it has been reported that the controllers are able to handle severe cases of measurement noise, as shown by (Gravdahl et al., 2002), (Bøhagen, 2007) and (Grong and Kylling, 2008). The measurement delay makes the controller unaware of the current state of the compressor, which means the controller is not able to take the required action fast enough to keep the compressor out of surge. This is the main problem with both active surge controllers being considered in this thesis. All types of flow meters are encumbered with certain delays from the actual flow being measured and delivered to the control system. $50ms$ does not appear significant, but is nevertheless considerable compared to the dynamics of the system. Before any of the solutions will be implemented in an industrial processing system, this problem must be addressed. A possible solution to this problem can be discussed later on. Another problem regarding the flow measurement is that in research, mass flow measurements are used, while in the industry volume flow is the preferred flow measurement parameter. This is because the exact gas composition must be known to measure the mass flow. This requires some kind of analysis of the gas flow, and it can take a considerably amount of time to obtain the information. Therefore, this information is not readily available for a control system. The equations for the controllers must be transformed to handle volume flow. This has, as far as the work with this thesis has uncovered, never been done.

The CCV solution requires a valve to be placed between the compressor and the plenum volume, as seen from Figure 3.1. This means that a compressor must be constructed with this in mind, and that retrofitting existing compressors with a CCV is difficult. In addition, the valve will change the behavior of the system, requiring a

re-tuning of the control system as well as the implementation of the CCV-controller itself. The drive torque solution requires that the drive system for the compressor is electrically driven. Most drive systems for compressors on offshore platforms are driven by gas turbines, which have slower response times compared to electrical drives. But replacing gas turbines with electrical drive is an ongoing discussion in the industry. This is not due to insufficient surge control, but because the gas turbines pollute, and have considerably CO_2 emissions. In addition, natural gas is used as fuel, rather than being sold or pumped back into the reservoir to increase the oil production. Rising gas prices and environmental awareness can thus push the replacement of gas turbines with electrical drive, provided that the electricity comes from renewable energy sources. The compressor system will still need a re-tuning, but compared to the CCV, electrical drive is more relevant for industrial use today than a CCV. This is mainly because the electrical drive already is a popular option.

Discussions with Professor Gravdahl and employees at Siemens Oil and Gas Offshore, Technology and Innovation Trondheim have brought up another problem regarding the CCV. The compressor used in this thesis (which is the same as the one used by (Gravdahl and Egeland, 1999)) and the compressor used by (van Helvoirt, 2007) are relatively small compared to industrial compressors found on offshore platforms. This difference is discussed in (Grong and Kylling, 2008) and (Grong, 2008). In a lab-scale compressor the CCV is relatively small in size, but needs to be fast acting in order to keep the compressor out of surge. (van Helvoirt, 2007) realized the need for constructing a new fast-acting valve to meet the requirements of the control system. This means the design of the valve itself is a challenge. And during the discussions it became clear that for an industrial compressor, the sheer size of the valve will make construction very difficult, since it also must be fast acting. Partly because of the problems related to the CCV, Professor Gravdahl has in resent years focused on the drive torque solution. The opinions of Professor Gravdahl and Siemens are very strong arguments against the use of CCV. Based on the above considerations, it is therefore concluded that the most promising solution for active surge control is the drive torque actuation and this should thus be the focus for further research.

5.2 State observer as a possible solution for measurement delay

As illustrated in the previous section, measurement delay on the flow measurement to the surge controller can make the compressor enter surge. This must be addressed before an active surge controller can be implemented in an industrial compressor system. In (Bøhagen, 2007) a possible solution is suggested. The use of observers

can compensate the measurement delay. The general form of the suggested observer can be found in (Fan and Arcak, 2003) and (Arcak and Kokotović, 2001). The model used for observer design is:

$$\dot{x} = Ax + G\gamma(\underbrace{Hx}_{v}) + \varrho(u, y) \tag{5.1}$$

$$y = [y_1\ y_2]^T = [Cx\ h(u, x)]^T \tag{5.2}$$

where $x \in R^n$,$u \in R^m$, $y_1 \in R^{r_1}$, $y_2 \in R^{R_2}$ and $\gamma : R^P \rightarrow R^P$. This structure ensures that the unmeasured states enter the compressor dynamics through the linear mapping Ax and the nonlinear mapping $\gamma(Hx)$. The mapping γ is assumed to satisfy the sector property given as:

$$(v - w)^T(\gamma(v) - \gamma(w)) \geq 0 \forall v, w \in R^P \tag{5.3}$$

The observer proposed for the system in Equation 5.1 and Equation 5.2 is:

$$\dot{\hat{x}} = A\hat{x} + G\gamma(\underbrace{H\hat{x} + K_2(C\hat{x} - y_1)}_{w}) + \varrho(u, y) + K_1(C\hat{x} - y_1) \tag{5.4}$$

Define now $e = x - \hat{x}$. Consider then the Lyapunov function candidate:

$$V(e) = e^T P e \tag{5.5}$$

where $P = P^T$ is positive definite. The time derivative of Equation 5.5 can be formulated as:

$$\dot{V}(t, e) \leq -2e^T Q_1 e - 2(v - w)^T Q_2(\gamma(v) - \gamma(w)) \tag{5.6}$$

provided that the linear matrix inequality (LMI)

$$\begin{bmatrix} (A + K_1C)^T P + P(A + K_1C) + Q - 1 & PG + (H + K_2C)^T Q_2 \\ G^T P + Q_2(H + K_2C & 0 \end{bmatrix} \leq 0 \tag{5.7}$$

is satisfied. The complete proof can be found in the appendix of (Bøhagen, 2007). The stability properties of the system is now given by the matrixes Q_1 and Q_2. If Q_1 is required to be positive definite, and Q_2 is chosen as the identity matrix, Equation 5.5, Equation 5.6 and Equation 5.7 ensure that $e = 0$ is exponentially stable. The observer gain K_2 can be found from the LMI, and K_1 calculated using P^{-1}, which exists because $P > 0$. For more information about calculating the gain matrices K_1 and, reference is made to (Bøhagen, 2007). The LMI can be investigated using the MATLAB function *feasp*.

5.2.1 Observer for pressure and mass flow

In this section an observer for the system from Equation 3.7 with the drive torque controller is derived and tested. From Equation 3.3 and Equation 3.4 it can be seen that the mass flow appears linearly in the pressure dynamics, through p_p in the mass flow dynamics and in the impeller speed dynamics through τ_c. The pressure dynamics provide more information about the mass flow because the absolute function for the mass flow in τ_c removes the sign of the mass flow. This is because the pressure dynamics take the sign of the mass flow into consideration. These considerations allow an observer to be proposed. The proposed observer, being adopted from (Bøhagen, 2007), is modified to fit the model used in this thesis.

Proposition 5.1. *The observer*

$$A = \begin{bmatrix} 0 & \frac{a_{01}^2}{V_p} \\ -\frac{A}{L} & -c_2 \end{bmatrix},\ G = \begin{bmatrix} -1 & 0 \\ 0 & 1 \end{bmatrix},\ H = \begin{bmatrix} 1 & 0 \\ 0 & 1 \end{bmatrix},\ C = \begin{bmatrix} 1 & 0 \end{bmatrix}$$
$$\gamma = \begin{bmatrix} \frac{a_{01}^2}{V_p} m_{out}(w_1) \\ c_2 w_2 \end{bmatrix}, \varrho = \begin{bmatrix} 0 \\ \frac{A}{L}\Psi_c(t) p_{01} \end{bmatrix}$$

where $c_2 \geq 0$, is exponentially stable if the LMI is solvable with $Q_2 = diag\{q_{21}, q_{22}\} > 0$.

Proof:

Equation 3.4 and Equation 3.3 give the pressure and mass flow dynamics. For convenience, define:

$$x_1 = p_p, x_2 = m, x_3 = U_1, u = \tau_l \tag{5.8}$$
$$k_1 = \frac{a_{01}^2}{V_p}, k_2 = \frac{A}{L}, k_3 = \frac{1}{I}, k_4 = k_l, k_5 = p_{01}, k_6 = k_c, k_7 = k_f \tag{5.9}$$
$$f_1(x_1) = \text{sgn}(x_1 - k_5)\sqrt{|x_1 - k_5|} \tag{5.10}$$
$$f_2(x_2, x_3) = \Psi_c(x_2, x_3) \tag{5.11}$$
$$f_3(x_2, x_3) = |x_2| x_3 \tag{5.12}$$

Available measurements are $y = \{x_1, x_3, f_2\}$. By using Equations 5.8 to 5.11 in combination with Equation 3.4 and Equation 3.3 the dynamic model can be expressed

as:

$$\begin{aligned}\begin{bmatrix}\dot{x}_1\\ \dot{x}_2\end{bmatrix} &= \begin{bmatrix}0 & k_1\\ -k_2 & 0\end{bmatrix}\begin{bmatrix}x_1\\ x_2\end{bmatrix} + \begin{bmatrix}-k_1k_4f_1(x_1)\\ 0\end{bmatrix} + \begin{bmatrix}0\\ k_2f_2(x_2,x_3)\end{bmatrix}\\ &= \begin{bmatrix}0 & k_1\\ -k_2 & -c_2\end{bmatrix}\begin{bmatrix}x_1\\ x_2\end{bmatrix} + \begin{bmatrix}-k_1k_4f_1(x_1)\\ c_2x_2\end{bmatrix} + \begin{bmatrix}0\\ k_2f_2(x_2,x_3)\end{bmatrix}\\ &= \underbrace{\begin{bmatrix}0 & k_1\\ -k_2 & -c_2\end{bmatrix}}_{A}\begin{bmatrix}x_1\\ x_2\end{bmatrix} + \underbrace{\begin{bmatrix}-1 & 0\\ 0 & 1\end{bmatrix}}_{G}\underbrace{\begin{bmatrix}k_1k_4f_1(x_1)\\ c_2x_2\end{bmatrix}}_{\gamma} + \underbrace{\begin{bmatrix}0\\ k_2f_2(x_2,x_3)\end{bmatrix}}_{\varrho} \end{aligned} \tag{5.13}$$

$$y_1 = \underbrace{\begin{bmatrix}1 & 0\end{bmatrix}}_{C}\begin{bmatrix}x_1\\ x_2\end{bmatrix} \tag{5.14}$$

where $c_2 \geq 0$ is a design constant, $\gamma(v_1, v_2) = [\gamma_1(v_1)\ \ \gamma_2(V_2)]^T$ and $v = [x_1\ x_2]^T$. From Equation 5.10 it can be recognized that Equation 5.3 holds for $\gamma_1(v_1)$, and because $c_2 \geq 0$, it also holds for $\gamma_2(v_2)$. This means that for $Q_2 = diag\{q_{21}, q_{22}\}$ due to the decomposition of γ. □

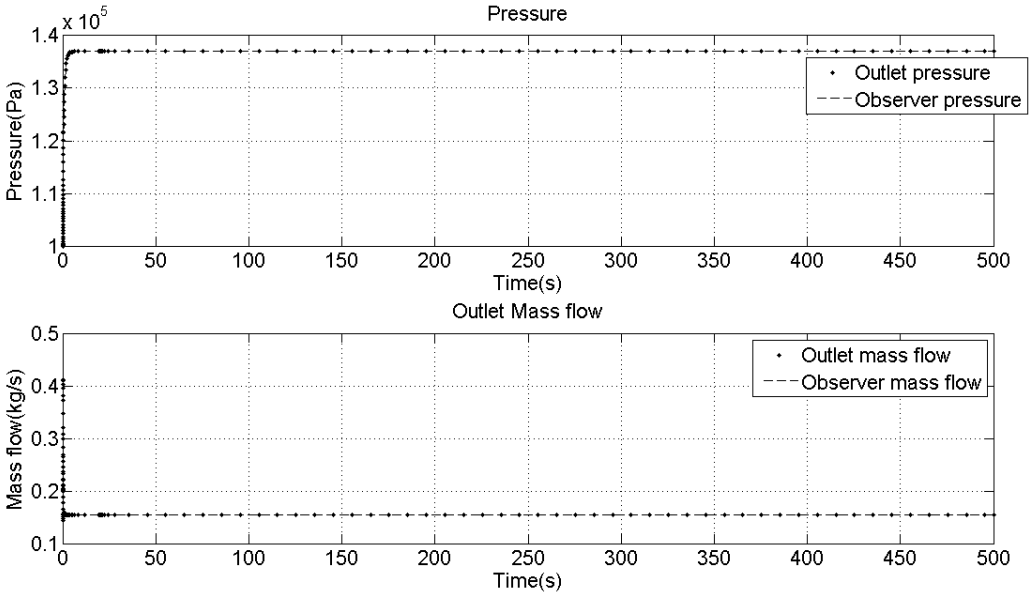

Figure 5.1: Comparison of outlet pressure and mass flow with corresponding outputs from the observer.

Figure 5.1 shows the outlet pressure and mass flow of the compressor plotted together with the corresponding outputs from the observer. The simulation is run

with the observer outputs as inputs to the controllers. Because of the lack of a start-up routine, which is present in a real compressor, a delayed switch of $0.5s$ is imposed on the controller inputs. This means that in the beginning the controllers are fed inputs directly from the model, but after $0.5s$ it only receives inputs from the observer. A measurement delay of $4s$ is added to the mass flow measurement. This is, however, not sufficient to make the compressor enter surge, as the observer tracks the model very well. This can be seen from the plots in Figure 5.1. The only clear deviation is that the mass flow observer does not contain the spike at the beginning. But this does not affect the overall performance of the controllers. However, this observer does not solve the problem of measurement delay. This becomes obvious if a measurement delay is added to the plenum pressure measurement, which is assumed to be available. The surge controller will then no longer be able to keep the compressor out of surge. This limits the use of this observer. In (Grong and Kylling, 2008) the practical implications of this is described further.

5.2.2 Full order observer

In this section an observer for pressure, mass flow and engine speed will be presented. The observer is from (Bøhagen, 2007), modified to fit the model used in this thesis.

Proposition 5.2. *The observer:*

$$A = \begin{bmatrix} 0 & \frac{a_{01}^2}{V} & 0 \\ -\frac{A}{L} & -c_2 & 0 \\ 0 & -c_3 & -\frac{k_f D - 1}{2I} \end{bmatrix},\ G = \begin{bmatrix} -1 & 0 & 0 & 0 \\ 0 & 1 & 1 & 0 \\ 0 & 0 & 0 & -1 \end{bmatrix},\ H = \begin{bmatrix} 1 & 0 & 0 \\ 0 & 1 & 0 \\ 0 & 1 & 0 \\ 0 & 0 & 1 \end{bmatrix}$$

$$C = \begin{bmatrix} 1 & 0 & 0 \\ 0 & 0 & 1 \end{bmatrix},\ \varrho = \begin{bmatrix} 0 \\ -c_3 U_1 \\ \frac{D_1}{2I} u + c_4 U_1^3 \end{bmatrix},\ \gamma = \begin{bmatrix} \frac{a_{01}^2}{V} m_{out}(w_1) \\ \frac{A}{L} \Psi_c(w_2, U_1) p_{01} + c_{21} w_2 \\ c_{22} w_3 + c_3 w_4 \\ \frac{D_1}{2I} \tau_c(w_3, w_4) - c_3 w_3 + c_4 w_4^3 \end{bmatrix}$$

$$c_2 = c_{21} + c_{22},\ c_{22} c_4 > \frac{k_c^2 D_1^2}{I^2 24},$$

and c_{21} sufficiently large, is exponentially stable if the LMI is solvable with $Q_2 = diag\{q_{21}, q_{22}, q_{22}, q_{23}\} > 0$.

Proof:

With the notation from Equations 5.8 to 5.12, the available measurements are $y =$

$\{x_1, x_3, f_2\}$. The model in Equation 3.4 and Equation 3.3 can now be expressed as:

$$\begin{aligned}
\begin{bmatrix}\hat{x}_1\\ \hat{x}_2\\ \hat{x}_3\end{bmatrix} &= \begin{bmatrix} 0 & k_1 0 & \\ -k_2 & 0 & 0 \\ 0 & 0 & -k_3k_7\end{bmatrix}\begin{bmatrix}x_1\\ x_2\\ x_3\end{bmatrix} + \begin{bmatrix} -k_1k_4f_1(x_1)\\ k_2f_2(x_2,x_3)\\ -k_3k_6f_3(x_2,x_3)\end{bmatrix} + \begin{bmatrix}0\\0\\k_3u\end{bmatrix}\\
&= \begin{bmatrix} 0 & k_1 & 0 \\ -k_2 & -c_2 & 0 \\ 0 & -c_3 & -k_3k_7\end{bmatrix}\begin{bmatrix}x_1\\ x_2\\ x_3\end{bmatrix} + \begin{bmatrix} -k_1k_4f_1(x_1)\\ k_2f_2(x_2,x_3)+c_2x_2+\alpha_2(y)\\ -k_3k_6f_3(x_2,x_3)+c_3x_2+\alpha_3(y)\end{bmatrix}\\
&\quad + \begin{bmatrix}0\\ -\alpha_2(y)\\ k_3u-\alpha_3(y)\end{bmatrix}\\
&= \underbrace{\begin{bmatrix} 0 & k_1 & 0 \\ -k_2 & -c_2 & 0 \\ 0 & -c_3 & -k_3k_7\end{bmatrix}}_{A}\begin{bmatrix}x_1\\ x_2\\ x_3\end{bmatrix} + \underbrace{\begin{bmatrix}0\\ -\alpha 2(y)\\ k_3u-\alpha_3(y)\end{bmatrix}}_{\varrho}\\
&\quad + \underbrace{\begin{bmatrix}-1 & 0 & 0 & 0\\ 0 & 1 & 1 & 0\\ 0 & 0 & 0 & -1\end{bmatrix}}_{G}\underbrace{\begin{bmatrix} k_1k_4f_1(x_1)\\ k_2f_2(x_2,x_3)+c_{21}x_2\\ c_{22}x_2+\alpha(y)\\ k_3k_6f_3(x_2,x_3)-c_3x_2-\alpha_3(y)\end{bmatrix}}_{\gamma}
\end{aligned} \tag{5.15}$$

$$y_1 = \underbrace{\begin{bmatrix}1 & 0 & 0\\ 0 & 0 & 1\end{bmatrix}}_{C}\begin{bmatrix}x_1\\ x_2\\ x_3\end{bmatrix} \tag{5.16}$$

The parameters c_2x_2, c_3x_2, $\alpha_2(y)$ and $\alpha_3(y)$ are added and subtracted in Equation 5.15 for design freedom. c_2 is defined such that $c_2 = c_{21} + c_{22}$. An appropriate expression for the term $(v-w)^T(\gamma(v)-\gamma(w))$ is:

$$\begin{aligned}
(v-w)^T(\gamma(v)-\gamma(w)) &= (v_1-w_1)(\gamma_1(v_1)-\gamma_1(w_1))\\
&\quad + (v'-w')^T(\gamma'(v')-\gamma'(w'))\\
&\quad + (v''-w'')^T(\gamma''(v'')-\gamma''(w''))
\end{aligned} \tag{5.17}$$

where

$$\gamma_1(v_1) = k_1k_4f_1(x_1) \tag{5.18}$$

$$\gamma'(t,v') = k_2f_2(x_2,x_3) + c_{21}x_2 \tag{5.19}$$

$$\gamma''(v'') = \begin{bmatrix} c_{22}x_2+\alpha_2(y)\\ k_3k_6f_3(x_2,x_3)-c_3x_2-\alpha_3(y)\end{bmatrix} \tag{5.20}$$

$v_1 = x_1$, $v' = x_2$ and $v'' = \begin{bmatrix} x_2 & x_3 \end{bmatrix}^T$. This leads to:

$$v = \begin{bmatrix} v_1 & v'^T & v''^T \end{bmatrix}^T = \begin{bmatrix} v_1 & v_2 & v_3 & v_4 \end{bmatrix}^T = \begin{bmatrix} x_1 & x_2 & x_3 & x_4 \end{bmatrix} \tag{5.21}$$

Equation 5.21 defines the matrix H. Equation 5.10 ensures that Equation 5.3 holds for Equation 5.18. For Equation 5.17 to be positive semi definite the following requirement must be fulfilled:

$$k_2 \frac{\delta f_2(a, x_3)}{\delta a}\bigg|_L + c_2 \geq 0 \Rightarrow \frac{\delta f_2(a, x_3)}{\delta a}\bigg|_L \leq -\frac{c_2}{k_2} \tag{5.22}$$

where a is evaluated at some point on the line segment L joining v_2 and w_2 using the mean value theorem. Equation 5.22 gives:

$$c_{21} > 0 \tag{5.23}$$

This will ensure that Equation 5.4 holds for Equation 5.20. The choices of:

$$c_{22} > 0 \tag{5.24}$$
$$\alpha_2(y) = c_3 x3 \tag{5.25}$$
$$\alpha_3(y) = -c_4 x_3^3 \tag{5.26}$$
$$c_{22} c_4 > \frac{k_3^2 k_6^2}{12} \tag{5.27}$$

guarantees that Equation 5.4 holds for Equation 5.21. The decomposition of γ then allows for $Q_2 = \{q_{21}, q_{22}, q_{22}, q_{23}\}$. □

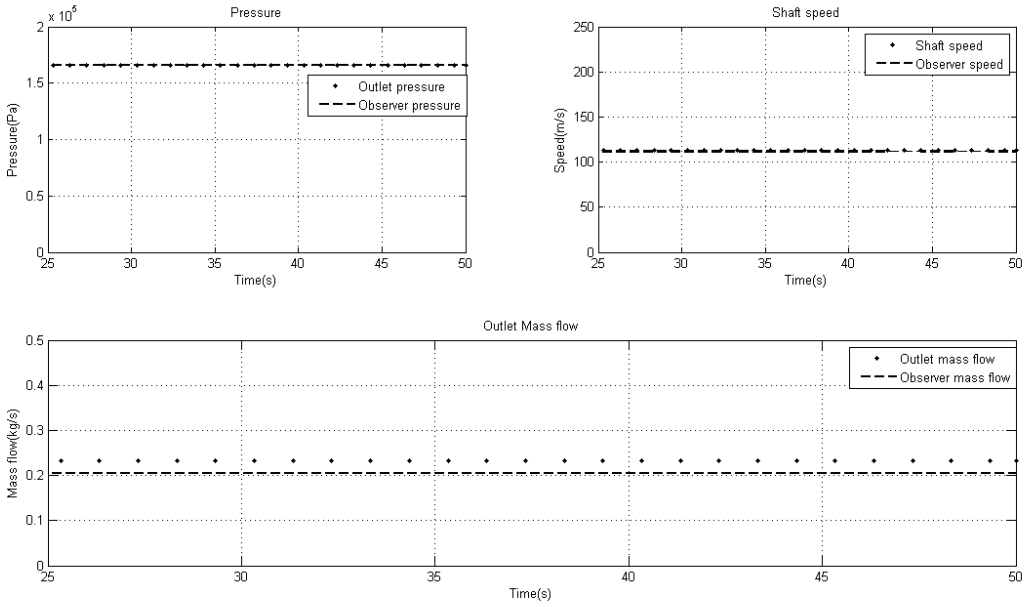

Figure 5.2: Comparison of outlet pressure, mass flow and shaft speed with corresponding outputs from the observer.

Figure 5.2 shows a comparison of outlet pressure, mass flow and shaft speed with corresponding outputs from the observer. This is after the stationary values have been reached. It can be seen from the mass flow plot that the observer deviates about 10 % from the actual value. Despite the efforts made to tune the parameters, this stationary deviation persists. This problem is confirmed by (Bøhagen, 2007). The observer in the current form is therefore not able to compensate the measurement delay.

Still, the observer represents a very promising solution to the measurement delay problem. The simulations in Figure 5.1 and Figure 5.2 were carried out without any measurement noise. If measurement noise had been included, the deviations would have been greater. A more thorough testing of different types of observers is carried out in (Bøhagen, 2007). The performance is reasonable, but the mass flow can deviate as much as 10% from the actual mass flow. (Bøhagen, 2007) also comments that the observers currently only are valid in a limited domain of the state space. More specifically, the impeller speed and plenum pressure must be positive. Because of the lack of studies of observers for mass flow in centrifugal compressors, this is certainly a field requiring more focus in the future if an active surge controller shall become commercially available.

Chapter 6

Concluding remarks and suggestions for further research

6.1 Conclusions

The basic conclusions that can be drawn from this thesis can be summarized as follows:

- A physical model for the compressor characteristics is of limited use. This is because of the required information being needed for the model, which must be obtained either from data sheets or by parameter estimation based on the information provided by the manufacturer. The performance of the physical model implemented in this thesis is good, but this is because the compressor being studied is relatively small and well documented. The physical model is best suited when used for research on specific parts of a compressor system, such as active surge controllers.

- On the other hand, the 4^{th}-order polynomial method is shown to be very easy to implement in a computer program. In this case the extracted points from the compressor characteristic are fed into an algorithm which then calculates the polynomials. The short calculation time being observed means that this solution can be useful in an online environment, where new compressor characteristics must be calculated fast due to rapid changes in the processing system. However, a requirement is that the initial polynomial coefficients must be calculated beforehand. The indications are that the 4^{th}-order polynomial method will perform best in an online simulation environment.

- The table lookup method also performs well, but the initial calculations being needed to obtain the extra speed-lines are shown to be very time-consuming.

This means that for an online system, all the required speed-lines must be known in advance, which is not always the case. For research applications, it is a great advantage that the table lookup method provides a very good representation of both single and multistage compressors. The time-consuming initial calculations are something that normally needs to be be done just once for a given compressor characteristic. This suggests that the table lookup method is the best solution for representing compressor characteristics in research based work.

- Another approach for representing the compressor characteristics in a dynamic model is to use parameter identification. This is a relatively new field in compressor modeling, but the indications are that this can be a better alternative than the normal tuning of a compressor model. The approach is currently able to determine two separate compressor model parameters independently. Alternatively, the same parameters must be either measured or approximated using an optimization algorithm. Parameter identification can extend the use of a physical model for the compressor characteristics because the required system parameters then more readily can be identified. However, more work is needed before this method can compete with the other methods mentioned above.

- It is verified that an active surge controller based on a close coupled valve (CCV) solution is able to keep the compressor out of surge, even if the compressor is operating within the unstable region of the compressor characteristic. This is also the case for an active surge controller based on drive torque actuation. Simulations with both controllers in use show that they perform well.

- Based on simulations and other considerations for the two active surge controllers, it is concluded that the drive torque solution is more promising than the CCV solution, and should therefore be the focus for further studies. Both types of controllers seek to solve the same problem. The drive torque solution requires electrical drive for the compressor. The replacement of gas turbines with electrical drive is already an ongoing discussion in the industry because of better engine control and environmental issues. On the other hand, the CCV solution needs to be included in the compressor design from the beginning, thereby making retrofitting very difficult. In addition, the CCV solution requires that a very large, fast-acting valve is developed, whereas complete engine control for electrical drives can be regarded more as commodity.

- The major problem with both active surge controllers is that they do not tolerate much delay in the compressor flow measurements. A measurement delay will make the controllers unable to react fast enough to changes occurring inside the

compressor, which, in turn, will force the compressor to enter surge. A possible solution to this problem is to develop a state observer for the compressor system. The two observers being studied in the present thesis have proved to function well from a mathematical point of view, but perform inadequately following implementation in SIMULINK.

6.2 Suggestions for further research

Of the three methods which have been used in this thesis for representing the compressor characteristics, the table lookup method is the best one with respect to accuracy. However, the method has proved to be very slow regarding computational time. This is because it relies on complex geometrical calculations to obtain the extra speed lines. An improvement of the algorithm used in these calculations can increase its efficiency. This will, in turn, make the method more useful, both in online and offline simulations of compressor systems.

Since the parameter identification in compressors is a relatively new and unexplored research field, it would be interesting to further investigate the possibilities of using this approach in compressor modeling. For example, the work done by (van Helvoirt et al., 2005) can be extended to enable the detection of multiple parameters independently. The same approach can also be used along with a physical compressor model to obtain the design parameters of the compressor, instead of employing the parameter optimization method used in (Grong and Kylling, 2008) and (Grong, 2008).

Based on the observation that the drive torque actuation is the most promising solution for active surge control, this is an obvious field for further research. In the past, most of the testing of this controller is done on small-scale research compressors. It would thus be fruitful to carry out studies on larger compressors in order to evaluate the performance of the controllers in industrial processing systems. Large-scale tests are important in order to demonstrate the benefits of using active surge control in the processing industry.

Before an active surge controller can be adopted by the industry, the problem of internal flow measurements must be solved. Firstly, most industrial compressor systems measure volume flow, and not mass flow, as normally done in research work. Since mass flow measurements require knowledge of the gas composition (which is difficult in an offshore processing system), the active surge controller must handle volume flow. Therefore, Professor Gravdahl has addressed the need for transforming the physical model of the compressor to handle volume flow. This refers to the com-

pressor model described in (Gravdahl and Egeland, 1999) and in the present thesis. These transformations would require a large amount of work, but it is uncertain in which way this affects the performance of the controllers.

The other problem with mass flow measurements is the one related to the measurement delay. It is reasonable to assume that an active surge controller based on volume flow measurement will face this problem. As discussed in this thesis, one possible solution is to use state observers to compensate the measurements. But the work done on nonlinear observers for compressor systems is strongly limited and will definitely need to be further investigated in the future.

Bibliography

ABB Research Ltd (2000). *Kompressorstyring*. Billingstad, Norway. Norwegian patent. Patent number: NO20005642.

Arcak, M. and Kokotović, P. (2001). Observer-based control of systems with slope-restricted nonlinearities. *IEEE Transactions on Automatic Control*, 46:1146–1150.

Asheim, H. and Hvidsten, R. (1991). *Plattformens hovedsystemer*. Vett og Viten. Norwegian.

Bloch, H. P. (2006). *A practical guide to compressor technology*. John Wiley & Sons, Inc, Hoboken, New Jersey.

Bøhagen, B. (2007). *Active surge control of centrifugal compression systems*. PhD thesis, Norwegian University of Science and Technology, Trondheim, Norway.

Boyce, M. P. (2003). *Centrifugal Compressors: A Basic Guide*. Pennwell Books.

Cumpsty, N. A. (1989). *Compressor Aerodynamics*. Longman.

de Jager, B. (1995). Rotating stall and surge control: A survey. In 34^{th} *IEEE Conf. On Decision and Control*, pages 1857–1862, New Orleans, LA, USA.

Erickson, C. E. (2008). Centrifugal Compressor Modeling Development and Validation for a Turbocharger Component Matching System. Master's thesis, Kansas State University, Manhattan, Kansas, USA.

Fan, X. and Arcak, M. (2003). Observer design for systems with multivariable monotone nonlinearities. *System & Control Letters*, 50:319–330.

Ferguson, T. B. (1963). *The centrifugal compression stage*. Butterworths, London.

Gravdahl, J. T. and Egeland, O. (1999). *Compressor Surge and Rotating Stall: Modeling and Control*. Springer Verlag, London.

Gravdahl, J. T. and Egeland, O. (2002). *Modeling and Simulation for Automaitc Control*. Marine Cybernetics AS, Trondheim, Norway.

Gravdahl, J. T., Egeland, O., and Vatland, S. O. (2002). Drive torque actuation in active surge control of centrifugal compressors. *Automatica*, 38:1881–1893.

Greitzer, E. M. (1976). Surge and Rotating stall in axial flow compressors, Part 1:Theoretical compressor system model. *Journal of Engineering for Power*, 98:190–198.

Grong, T. S. (2008). *Modeling of compressor train*. Norwegian University of Science and Technology. Project Report.

Grong, T. S. and Kylling, Ø. W. (2008). Compressor modeling and control. Technical report, Siemens Oil and Gas Offshore - Technology and Innovation.

Khalil, H. K. (2002). *Nonlinear Systems*. Prentice Hall, New Jersey, USA.

Kylling, Ø. W. (2008). *Modelling and control of an offshore oil and gas production plant*. Norwegian University of Science and Technology. Project Report.

McKee, R. J., Edlund, C. E., and Pantermuehl, P. J. (2000). Development on an active surge control system. Technical report, Mechanical and Materials Engineering Division, Southwest Research Institute.

Moore, F. K. and Greitzer, E. M. (1986). A theory of post stall transient in axial compression systems: Part I– development of equations. *ASME J. Engineering for Gas Turbines and Power*, 108:68–76.

Neverlý, J., Marek, J., Vargovčík, L., and Oldřich, J. (2008). Centrifugal compressor dynamics and software system for surge control. In *The* 20^{th} *International Conference on Hydraulics and Pneumatics*, Prague, Czech Republic.

Nisenfeld, A. E. (1982). *Centrifugal compressors: principles of operation and control*. Instrument society of America.

Pampreen, R. C. (1973). Small turbomachinery compressor and fan aerodynamics. *Journal of Engineering for Power*, 95:251–256.

Siemens (2000). *ConSi MAPS, Multicondition Antisurge Protection System, Functional Description*, 2^{th} edition.

Siemens (2008). Course in Topside Processing. Powerpoint presentation.

Tipler, P. A. and Mosca, G. (2004). *Physics for scientists and engineers, Extended*. W.H. Freeman and Company, 5^{th} edition.

van Helvoirt, J. (2007). *Centrifugal Compressor Surge : Modeling and Identification for Control*. PhD thesis, Technische Universiteit Eindhoven, Eindhoven, The Netherlands.

van Helvoirt, J., de Jager, B., Steinbuch, M., and Smeulers, J. (2005). Modeling and Identification of Centrifugal Compressor Dynamics with Approximate Realizations. In *2005 IEEE International Conference on Control Applications*, pages 1441–1447, Toronto, Canada.

Watson, N. and Janota, M. S. (1982). *Turbocharching the internal combustion engine*. MacMillan.

White, F. M. (2003). *Fluid Mechanics*. McGraw-Hill Higher Education, New York, USA, 5^{th} edition.

Willems, F. P. T. (2000). *Modeling and Bounded Feedback Stabilization of Centrifugal Compressor Surge*. PhD thesis, Technische Universiteit Eindhoven, Eindhoven, The Netherlands.

Appendix A

Nomenclature

A.1 Greek uppercase

$\Delta h_{0c,ideal}$ Specific enthalpy without losses

Δh_{fd} Fluid friction loss at diffuser

Δh_{fi} Fluid friction loss at impeller

Δh_{id} Incidence loss at diffuser

Δh_{ii} Incidence loss at impeller

Δn Clearance, back-flow, volute and diffusion loss in centrifugal compressor

Ψ_{c0} Compressor shut off valve

Ψ_c Compressor characteristic

Ψ_e Compressor characteristic for equivalent compressor

Ψ_v Compressor characteristic for close coupled valve

A.2 Greek lowercase

β_{1b} Fixed impeller blade angle

β_{2b} Impeller backsweep angle

ω Rotor speed

ρ_{01} Constant stagnation inlet density

σ Slip factor

τ_c Compressor torque

τ_l Drive torque from motor

A.3 Latin uppercase

A_d Cross section area of diffuser

A_i Cross section area of impeller eye

C_{2a} Axial component of gas velocity at impeller tip

$C_{\theta 2}$ Gas velocity at impeller tip

C_h Surface friction loss coefficient

CCV Close coupled valve

D_1 Average inducer diameter

D_2 Impeller diameter at tip

D_{h1} Diameter at hub casing

D_{l1} Diameter at inducer tip

I Spool moment of inertia

L_c Length of compressor and duct

Q Heat flow

S Stress tensor

U_1 Tangential velocity at rotor

U_2 Impeller tip velocity

V_p Plenum volume

Re Fluid Reynolds number

A.4 Latin lowercase

a_{01}	Inlet stagnation sonic velocity
f	Friction factor
g	Acceleration of gravity
i	Number of impeller blades
k_l	Throttle gain
m	Compressor mass flow
m_l	Mass flow through throttle valve
m_s	Mass flow through recycle valve
m_w	Mol weight of gas
p_2	Pressure downstream of the compressor
p_p	Plenum pressure
ppm	Parts per million
z	Compressibility factor

Appendix B

Thermodynamics

The following information is from (Gravdahl and Egeland, 1999), (White, 2003), (Tipler and Mosca, 2004), (Bloch, 2006), (Bøhagen, 2007) and (van Helvoirt, 2007).

B.1 Thermodynamic property data

Properties of a system are macroscopic characteristics of a system. Mass, pressure, temperature, compressibility and energy are examples of such properties. Numerical values can be assigned to these properties without knowing the history of the system. Enthalpy is defined on a mass basis as:

$$h = u + p\rho^{-1} \tag{B.1}$$

where u is the specific internal energy, p is the pressure and ρ is the mass density. The denomination for h and u is $[J/kgK]$. The ratio of specific heats is defined as:

$$k = \frac{c_p}{c_v} \tag{B.2}$$

The specific heats are defined as:

$$\begin{aligned} c_v &= \left.\frac{\delta u(T,\rho)}{\delta T}\right|_{\rho} \\ c_p &= \left.\frac{\delta u(T,p)}{\delta T}\right|_{p} \end{aligned} \tag{B.3}$$

c_p is the specific heat capacity at constant pressure, whereas c_v is at constant volume. The SI unit for specific heat is $[J/kgK]$.

B.2 p-v-T relation for gases

The universal gas constant is defined as $\bar{R} = 8.314\,[J/kmolK]$. *For a specific gas the gas constant is:*

$$R = \frac{\bar{R}}{M} \tag{B.4}$$

where M *is the molecular weight of the gas. The compressibility factor for a gas is defined as:*

$$Z = \frac{p}{\rho RT} \tag{B.5}$$

B.3 Ideal gas model

If the compressibility factor is assumed equal to unity, the ideal gas law can be formulated as:

$$pV = \rho RT \tag{B.6}$$

The internal energy function for an ideal gas is only a function of its internal temperature. A complete model for an ideal gas becomes:

$$\begin{aligned} pv &= \rho RT \\ u(T,\rho) &= u(T) \\ h(u,p,\rho) &= h(T) = u(T) + RT \end{aligned} \tag{B.7}$$

For this model the specific heats as a function of temperature must be known. This information can be found in graphs, tables and equations. The ideal gas law is most accurate for mono-atomic gases at high temperatures and low pressures. When the gas is close to a phase change the deviations from an ideal gas becomes significant. A more accurate equation capturing deviations in molecular size and intermolecular forces are the van der Waals equation:

$$(p + \frac{a'}{v^2})(v - b') = kT \tag{B.8}$$

where p *is the fluid pressure,* V *is the total volume of the container containing the fluid divided by the total number of particles,* a' *is a measure of attraction between particles,* b' *is the average volume excluded from* V *by a particle,* k *is the Boltzmann's constant and* T *is the absolute temperature. The van der Waals equation is a better model than the ideal gas law, but requires more information about the specified gas' properties.*

B.4 Isentropic and polytropic process

The entropy of a system is a measure of the systems availability of energy. A high entropy in a system means that the system can do less useful work. It is a measure of the randomness of molecules in a system. In thermodynamics it is related to the second law of thermodynamics and the fundamental thermodynamic relation. Entropy states whether or not a change in an isolated system can happen spontaneously. A spontaneous change will increase the entropy of the system. An isentropic process is a process in which the entropy of the working fluid remains constant during the process. In the context of gas compression it means that no heat is transferred to the gas during the compression. The compression follows the equation

$$p_1 V_1^k = p_2 V_2^k \tag{B.9}$$

This is impossible to accomplish in a real compressor. The isentropic process is desirable for a compression system, and therefore cooling of the gas is normally done. In thermodynamics, a polytropic process is a process that obeys the relation:

$$PV^n = C \tag{B.10}$$

where P is the pressure, V is the volume, n is the polytropic index (can attain any real number) and C is a constant. Polytropic processes are internally reversible. A reversible process is a process in which the state of the working fluid and system surroundings can be restored to its original state. Complete reversibility implies no internal or mechanical friction. In addition, the temperature and pressure difference between the working fluid and the surroundings should be infinitively small. Because of this no physical process is reversible in practice. But polytropic efficiency is often provided by the compressor producers to specify how much of the energy being put into the compressor that is used to increase the pressure of the gas. Energy that are used to increase temperature of the gas is in reality a waste.

Let s denote specific entropy, u denote specific internal energy, $v = \frac{V}{m} = \rho^{-1}$ denote specific volume and $h = u + pv$ denote specific enthalpy. It can then be shown that:

$$ds = \frac{dQ}{T} \tag{B.11}$$

The differential form of the of the non-flow energy equation is:

$$dQ = du + pdv \tag{B.12}$$

Then it follows that:

$$\begin{aligned} Tds &= du + pdv \\ Tds &= dh - vdp \end{aligned} \tag{B.13}$$

If the specific heat capacities, c_p and c_v is held constant, Equation B.13 can be written:

$$\begin{aligned} Tds &= c_v dT + pdv \\ Tds &= c_p dT - vdp \end{aligned} \tag{B.14}$$

For an isentropic process, which is reversible and adiabatic, $ds = 0$, and:

$$\begin{aligned} dT &= -\frac{p}{c_v} dv \\ dT &= \frac{v}{c_p} dp \end{aligned} \tag{B.15}$$

It then follows that

$$\frac{dp}{p} = -k\frac{dv}{v} \tag{B.16}$$

where $k = \frac{c_p}{c_v}$ is the ratio of specific heats.

B.5 Compressor pressure rise

Here Equation 2.9 is derived.

$$\eta_i(m, U_1) = \frac{h_{2s} - h_{01}}{h_{02} - h_{01}} \tag{B.17}$$

is the compressor total to static isentropic efficiency. h_{2s} is the outlet static enthalpy with isentropic compression, h_{01} is the inlet stagnation enthalpy and h_{02} is the outlet stagnation enthalpy. By assuming perfect gas law, so that $h = Tc_p$ and c_p is constant. The efficiency now becomes:

$$\eta_i(m, U_1) = \frac{T_{2s} - T_{01}}{T_{02} - T_{01}} = \frac{\frac{T_{2s}}{T_{01}} - 1}{\frac{T_{02}}{T_{01}} - 1} \tag{B.18}$$

This can be modified by using the relation for isentropic compression:

$$\eta_i(m, U_1) = \frac{(\frac{p_2}{p_{01}})^{\frac{k-1}{k}} - 1}{\frac{T_{02}}{T_{01}} - 1} = \frac{T_{01}c_p((\frac{p_2}{p_{01}})^{\frac{k-1}{k}} - 1)}{c_p(T_{02} - T_{01})} \tag{B.19}$$

(Watson and Janota, 1982) show that for a radially vaned impeller the following holds:

$$\eta_i(m, U_1) = \frac{T_{01}c_p((\frac{p_2}{p_{01}})^{\frac{k-1}{k}} - 1)}{\Delta h_{0c,ideal}} \tag{B.20}$$

This can be rearranged to:

$$\frac{p_2}{p_{01}} = \left(1 + \frac{\eta_i(m, U_1)\Delta h_{0c,ideal}}{T_{01}c_p}\right)^{\frac{k}{k-1}} \tag{B.21}$$

Appendix C

Fluid dynamics

The following information is from (Gravdahl and Egeland, 1999), (White, 2003), (Tipler and Mosca, 2004), (Bloch, 2006), (Bøhagen, 2007) and (van Helvoirt, 2007).

C.1 Conservation laws

In this section the mass and momentum conservation laws on integral form will be presented. This is vital in every attempt of modeling a compressor system. Gauss' 2^{nd} theorem states that for a tensor field $\mathbf{F}$ *of any order, the region* V *within the closed surface* A *and the perpendicular unit vector* n *to this surface. An illustration of the gauss theorem can be found in Figure C.1.*

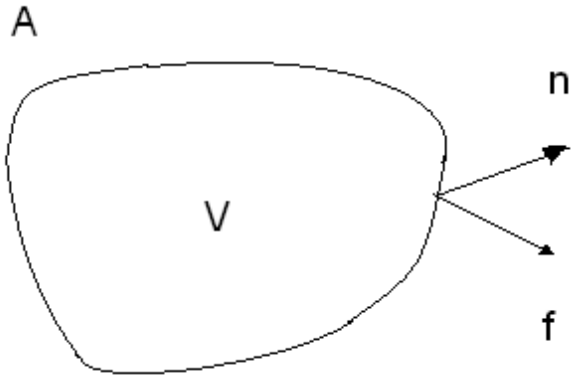

Figure C.1: Illustration of the Gauss 2^{nd} theorem.

$$\int_V \boldsymbol{\nabla} \cdot \boldsymbol{F} dV = \int_A \mathbf{n} \cdot \mathbf{F} dA \tag{C.1}$$

The complete proof of this theorem can be found in (White, 2003). The laws of conservation states that the net change of a property within a closed region is equal to the net flux of this property into the region. This is expressed by:

$$\frac{d}{dt} \int_{V(t)} \mathbf{F}(x,t) dV = \Upsilon(t) - \int_{B(t)} \mathbf{n}(t) \cdot \mathbf{F}(x,t) dB \tag{C.2}$$

In Equation C.2, $\mathbf{F}$*(x,t) is a tensor of any rank, V(t) is an arbitrary region and* $\Upsilon(t)$ *a general source term describing the generation of annihilation of* $\mathbf{F}$*(x,t), B(t) is the boundary over which* $\mathbf{F}$ *can enter or leave the region. Figure C.2 gives a graphical representation of the principle.*

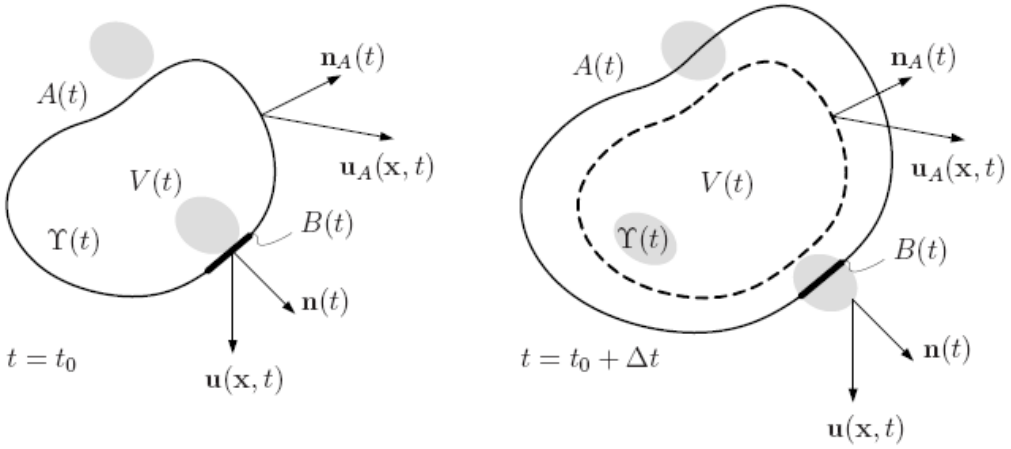

Figure C.2: Illustration of the principle of conservation.

By applying the generalized Leibniz theorem, Equation C.2 can be modified to:

$$\frac{d}{dt}\int\limits_{V(t)} \mathbf{F}(x,t)dV = \int\limits_{V(t)} \frac{\delta \mathbf{F}(x,t)}{\delta t}dV + \int\limits_{A(t)} \mathbf{F}(x,t)(\mathbf{n}_A(t)\cdot\mathbf{u}_A(x,t))d\mathcal{A} \tag{C.3}$$

where $\mathbf{n}_A$ *being the unit normal and* $\mathbf{u}_A$ *the velocity of the boundary surface A(t) of the region V(t). Normally,* $B(t) \subseteq A(t)$.

Given a material volume $V(t) = \mathcal{V}(t)$*, the surface* $\mathcal{A}(t)$ *will move with the medium, such that* $u_A(t) = u(x,t)$ *and* $\mathcal{B}(t) = \emptyset$*. A substitution in Equation C.2 and Equation C.3 gives:*

$$\frac{d}{dt}\int\limits_{V(t)} \boldsymbol{F}(x,t)d\mathcal{V} = \int\limits_{V(t)} \frac{\delta \boldsymbol{F}(x,t)}{\delta t}d\mathcal{V} + \int\limits_{A(t)} \boldsymbol{F}(x,t)(\boldsymbol{n}(t)\cdot\boldsymbol{u}(x,t))d\mathcal{A} = \Upsilon(t) \tag{C.4}$$

Equation C.4 is known as Reynolds transport theorem. The rate of increase of mass inside a material volume can be formulated inserting $textbfF(x,t) = \rho(x,t)$ *in Equation C.4. This gives:*

$$\frac{d}{dt}\int\limits_{\mathcal{V}(t)} \rho d\mathcal{V} = \int\limits_{\mathcal{V}(t)} \frac{\delta \rho}{\delta t}d\mathcal{V}(t) + \int\limits_{\mathcal{A}(t)} \rho(\boldsymbol{n}(t)\cdot\boldsymbol{u}(x,t))d\mathcal{A} = 0 \tag{C.5}$$

. It is assumed that $\Upsilon = 0$*, which means that no mass is generated. The dependencies of x and t will hereafter be omitted for simplicity. The surface integral from Equation*

C.5 can be transformed using the divergence theorem. This will result in a volume integral formulated as:

$$\int_{\mathcal{V}(t)} \frac{\delta \rho}{dt} d\mathcal{V} + \int_{\mathcal{V}(t)} \boldsymbol{\nabla} \cdot (\rho \boldsymbol{u}) d\mathcal{V} = \int_{\mathcal{V}(t)} \left(\frac{1}{\rho} \frac{Dp}{Dt} + \boldsymbol{\nabla} \cdot \boldsymbol{u} \right) d\mathcal{V} = 0 \tag{C.6}$$

Equation C.6 is the law of conservation of mass flow on integral form. Using the index notation the differential form of the continuity equation is:

$$\frac{\delta \rho}{\delta t} + \frac{\delta (\rho u_j)}{\delta x_j} = 0 \tag{C.7}$$

To introduce the law of conservation of momentum, $\boldsymbol{F}(x,t)$ can be replaced with the impulse density $\rho(x,t)\boldsymbol{u}(x,t)$. By substitution in the Reynolds transport theorem from Equation C.4 and using the divergence theorem yields

$$\int_{\mathcal{V}(t)} \left(\frac{\delta (\rho \boldsymbol{u})}{\delta t} + \boldsymbol{\nabla} \cdot (\rho \boldsymbol{u} u) \right) d\mathcal{V} = \Upsilon(t) \tag{C.8}$$

Again using index notation, the lefthand side of Equation C.8 can be rewritten as:

$$\frac{\delta (\rho u_i)}{\delta t} + \boldsymbol{\nabla} \cdot (\rho u_j u_i) = \rho \frac{\delta u_i}{\delta t} + u_i \frac{\delta \rho}{\delta t} + u_i \frac{\delta (\rho u_j)}{\delta x_j} + \rho u_j \frac{\delta u_i}{\delta x_j} = \rho \frac{\delta u_i}{\delta t} + \rho u_j \frac{\delta u_i}{\delta x_j} \tag{C.9}$$

The impulse in $\mathcal{V}(t)$ can in addition to be changed by a moving boundary, be changed by body and surface forces doing work on $\mathcal{V}(t)$. This means that $\Upsilon(t)$ is not always equal to zero. By considering gravity, pressure and stress forces the following expression is obtained:

$$\int_{\mathcal{V}(t)} \rho \frac{D\boldsymbol{u}}{Dt} = \int_{\mathcal{V}(t)} \rho g d\mathcal{V} - \int_{\mathcal{A}(t)} p \boldsymbol{n} d\mathcal{A} + \int_{\mathcal{A}(t)} \boldsymbol{n} \cdot S d\mathcal{A} \tag{C.10}$$

where g is the acceleration of gravity, p is the pressure and S is the stress tensor.A constitutive equation for a Newtonian fluid, to incorporate the relation between stress and deformation, can be expressed as:

$$\boldsymbol{S} = \mu \nabla^2 \boldsymbol{U} + \left(\kappa + \frac{1}{3} \mu \right) \boldsymbol{\nabla} (\boldsymbol{\nabla} \cdot \boldsymbol{u}) \tag{C.11}$$

By again using the divergence theorem, Equation C.10 can be written as:

$$\int_{\mathcal{V}(t)} \left(\rho \frac{D\boldsymbol{u}}{Dt} \right) d\mathcal{V} = \int_{\mathcal{V}(t)} (\rho g - \boldsymbol{\nabla} p + \boldsymbol{\nabla} \cdot \boldsymbol{S}) d\mathcal{V} \tag{C.12}$$

Equation C.12 is the law of conservation of momentum on integral form. In index notation it is written:

$$\rho\frac{Du_i}{Dt} = \rho g_i - \frac{\delta p}{\delta x_i} + \frac{\delta S_{ji}}{\delta x_j} \tag{C.13}$$

By substituting Equation C.11 into Equation C.13 will yield the so-called Navier-Stokes equation for motion of fluids.

C.2 Assumption of incompressible flow

The assumption of incompressible flow is not valid for flow with high Mach numbers. This will be illustrated with an example. The one-dimensional continuity equation for steady flow is:

$$u\frac{\delta\rho}{\delta x} + \rho\frac{\delta u}{\delta x} = 0 \tag{C.14}$$

The assumption of incompressible flow means:

$$u\frac{\delta\rho}{\delta x} \ll \rho\frac{\delta u}{\delta x} \tag{C.15}$$

or that:

$$\frac{d\rho}{\rho} \ll \frac{du}{u} \tag{C.16}$$

Using the relation $dp \simeq c^2 dp$ to estimate changes in pressure, it can be found from the momentum equation for an inviscid steady flow that:

$$udu = \frac{dp}{\rho} \tag{C.17}$$

The relation $dp \simeq c^2 dp$ is an approximation when the process is not isentropic. Comparison with Equation C.16states that changes in the density are negligible if:

$$\frac{u^2}{c^2} = M^2 \ll 1 \tag{C.18}$$

Equation C.18 states that the assumption of incompressible flow is only valid for sufficiently low Mach numbers.

Appendix D

Matlab files

D.1 Compressor simulation parameters

This is the constant file used in the simulation for the physical representation of the compressor characteristic, as well as for the two active surge controller and observers.

```
%Gas properties
a01 = 340; %speed of sound in gas(m/s)
p01 = 1e5; %Compressor inlet pressure(Pa)
T01 = 303.35; %Compressor inlet temperature(K)
cp = 1005; %specific heat capacity for constant pressure, property of gas(J/(kg*K))
    ro1 = 1.15; %Gas density(kg/m^3)
    Re = 100000; %Reynolds number()
    k = 1.4; %Gas constant ratio, cp/cv()

    %Compressor characteristics
    L = 1.253; %Length of compressor and duct(m)
    Vp = 0.21; %Plenum volume(m^3)
    kl = 0.0008; %Throttle gain, proportional to the throttle opening
    Dt1 = 0.074; %Impeller diameter at inducer tip(m)
    Dh1 = 0.032; %Impeller diameter at hub casing(m)
    D1 = 1/sqrt(2)*sqrt((Dt1)^2+(Dh1)^2); %Average diameter(m)
    Di = 0.02; %Mean hydraulic diameter of impeller(m)
    Dd = 0.02; %Mean hydraulic diameter of impeller(m)
    I = 0.001; %Moment of inertia for the compressor spool(kg*m^2)
    alfa1 = pi/2; %Flow angle at inducer, for alpha1 = pi/2 rad, assumed no pre-whirl
    A = ((pi*D1^2)/4)*4;
    Ai = ((pi*D1^2)/4); % Cross section area impeller(m^2)
```

```
Ad = ((pi*D1^2)/4); % Cross section area diffuser(m^2)
deltanbf = 0.03; %Back flow loss()
deltanv = 0.035; %Volute loss()
deltanc = 0; %Clearance loss()
deltand = 0; %Diffusion loss()
li = 0.053; %Mean channel length(m)
ld = 0.053; %Mean channel length(m)
beta1b = 0.61; %Impeller blade inlet angle()
Ch = 4*0.3164*(Re)^-0.25; %Friction loss coefficient()
kf = (Ch*li)/(2*Di*ro1^2*Ai^2*(sin(beta1b))^2)*4; %Friction loss impeller
kfd = (Ch*ld)/(2*Dd*ro1^2*Ad^2*(sin(beta1b))^2);%Friction loss diffuser
sigma = 0.9; %Slip factor()
D2 = 0.128; %Diameter of impeller tip(m)

%Controller parameters
kp = 0.1; %Controller proportional gain
ki = 0.07; %Controller integral gain
kd = 0; %Controller derivate gain
kv = 0.4; %Controller mass flow gain
N = 50000; %Desired setpoint for engine revolution(rpm)
U1 = (D1*pi*N)/60;
Ud = (D1*pi/60)*N; %Setpoint for shaft speed.

%mass controller
kim=80; %Controller proportional gain
kpm=10; %Controller integral gain
m0 = 0.3; %Setpoint for mass flow

%pressure controller
kpp= 0.0023; %Controller proportional gain
kip=0.004; %Controller integral gain
kdi = 0; %Controller derivate gain
p0 = 1.37e5; %Setpoint for pressure

%Torque controller
k1 = 0.1;
k2 = 0.07;
```

D.2 Observer parameters

In addition to the compressor parameters above, the observer matrices used in the simulations can be found below. The first set of parameters are for the reduced order observer and the second for the full order observer.

Constants reduced order observer:

```
%Observer parameter reduced order
c2 = 10.5;%0;
c3 = -10.9;%0.26;
c4 = -10.46;%0.46;
Am = [0, (cp^2)/Vp; -(A/L), -c2,];
G = [-1,0;0,1];
H = [1,0;0,1];
C = [1,0];
k1 = (cp^2)/Vp;
k2 = A/L;
k3 = 1/I;
k5 = p01;
k6 = 1;
k7 = 1.33e5;
K2 = [4.9e3;-2];
K1 = [-1.9e30;-1.1e-2];
```

Constants full order observer:

```
%Observer parameters full order
c21 = 1;
c22 = 0.6;
c2 = c21 + c22;
c3 = -1.26;
c4 = 1;
Am = [0, (cp^2)/Vp, 0; -(A/L), -c2, 0; 0, -c3,-(kf)/(I)];
G = [-1,0,0,0;0,1,1,0;0,0,0,-1];
H = [1,0,0;0,1,0;0,1,0;0,0,1];
C = [1,0,0;0,0,1];
k1 = (cp^2)/Vp;
k2 = A/L;
k3 = 1/I;
k5 = p01;
k6 = 1;
k7 = 1.33e5;
K2 = [1.2,1.2;1,1;1,1;1,1;1,1];%[1,1;1,1;1,1];
K1 = [-10,-10;-1e-5,-1e-5;-1.09e-3,-1.09e-3];
```